

Stable Anilinyl Radicals Coordinated to Nickel: X-ray Crystal Structure and Characterization

Amélie Kochem,^[a] Gisèle Gellon,^[a] Nicolas Leconte,^[a] Benoit Baptiste,^[a] Christian Philouze,^[a] Olivier Jarjayes,^[a] Maylis Orio,^[b] and Fabrice Thomas^{*,[a]}

Abstract: Two anilinosalen and a mixed phenol-anilinosalen ligands involving sterically hindered anilines moieties were synthesized. Their nickel(II) complexes **1**, **2**, and **3** were prepared and characterized. They could be readily one-electron oxidized ($E_{1/2} = -0.30, -0.26$ and 0.10 V vs. Fc^+/Fc , respectively) into anilinyl radical species $[\mathbf{1}]^+$, $[\mathbf{2}]^+$, and $[\mathbf{3}]^+$, respectively. The radical complexes are extremely stable and were isolated as single crystals. X-ray crystallographic structures reveal

that the changes in bond length resulting from oxidation do not exceed 0.02 \AA within the ligand framework in the symmetrical $[\mathbf{1}]^+$ and $[\mathbf{2}]^+$. No quinoid bond pattern was present. In contrast, larger structural rearrangements were evidenced for the unsymmetrical $[\mathbf{3}]^+$, with shortening of one $C_{\text{ortho}}-$

C_{meta} bond. Radical species $[\mathbf{1}]^+$ and $[\mathbf{2}]^+$ exhibit a strong absorption band at around 6000 cm^{-1} (class III mixed valence compounds). This band is significantly less intense than $[\mathbf{3}]^+$, consistent with a rather localized anilinyl radical character, and thus a classification of this species as class II mixed-valence compound. Magnetic and electronic properties, as well as structural parameters, have been computed by DFT methods.

Keywords: aminyl • aniline • ligands • nickel • radicals • X-ray diffraction

Introduction

The coordination chemistry of redox non-innocent ligands with d-transition metals has attracted a considerable interest during the past few years.^[1] The non-innocence of a ligand manifests when it is possible to differentiate the formal oxidation state of a given complex from its real (spectroscopic) one. A number of ligands are recognized as non-innocent in inorganic chemistry, for example, diimine,^[2] catechols,^[3] aminophenols,^[4] phenylene diamines,^[5] and phenols.^[6] Redox non-innocent ligands are also found in the active sites of several metalloproteins, whose archetypes are galactose oxidase (phenoxyl/phenolate couple)^[7] and cytochrome P450 (radical heme/heme couple).^[8] As electron reservoirs, they assist the metal ion in electron transfers during turnovers,^[9] providing an elegant strategy to overcome the inherent in-

ability of some earth-abundant transition-metal ions to accommodate multi-electron changes usual in biocatalysis.

Aminyl radicals are rather unstable species, which are involved in number of important chemical transformations.^[10–13] For instance, as reactants they readily abstract hydrogen atoms from organic substrates.^[11,12] They are also key intermediates in several reactions involving organic compounds, inorganic complexes, and metalloenzymes.^[13]

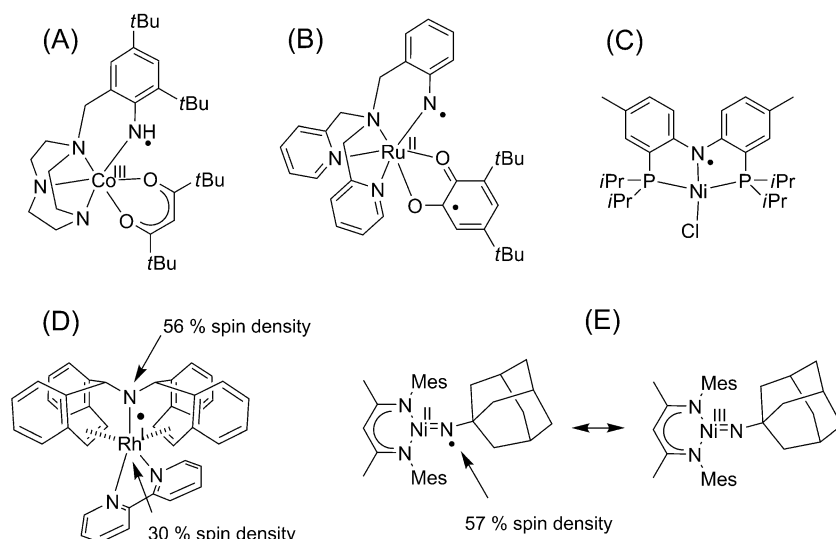
Persistent anilinyl (of formula $\text{PhNH}_2^{\cdot+}$ or PhNH^{\cdot}) or aminyl (of general formula $\text{R}_1\text{N}^{\cdot}\text{R}_2$) radicals are rather uncommon compounds.^[14] Consequently their use as a ligand in inorganic chemistry is very limited.^[11,15–20] In the early 2000s, Wieghardt et al. reported some cobalt and manganese complexes involving a coordinated anilinyl moiety, which was incorporated into a polydentate 1,4,7-triazacyclononane (TACN) scaffold (Scheme 1A).^[16] Tanaka et al. recently described a ruthenium(II) anilinyl radical complex issued from a tripodal ligand (Scheme 1B),^[17] whereas both Peters and Mindiola et al. synthesized aminyl complexes from a deprotonated diphenylamine (copper(I) and Ni^{II} complexes, respectively; the latter is shown in Scheme 1C).^[18]

Recently, a major advance was achieved in this field by Grützmacher et al., who successfully isolated coordinated $\text{R}_1\text{N}^{\cdot}\text{R}_2$ aminyl radicals as single crystals and reported their first structural characterization (Scheme 1D).^[11,19] At the same time Warren et al. (Scheme 1E), who were interested in nitrene transfer by metal complexes, described the compound depicted in Scheme 1E. This complex was described as a $\text{Ni}^{\text{III}}=\text{nitrene}$ species with a significant contribution of the Ni^{II} anilinyl electronic isomer.^[20] In Grützmacher's complex the aminyl nitrogen is coordinated to either a rhodium

[a] Dr. A. Kochem, G. Gellon, Dr. N. Leconte, Dr. B. Baptiste, Dr. C. Philouze, Dr. O. Jarjayes, Prof. Dr. F. Thomas
Département de Chimie Moléculaire
Chimie Inorganique Redox Biomimétique (CIRE)
UMR-5250, Université Joseph Fourier, BP 53
38041 Grenoble Cedex 9 (France)
Fax: (+33)476-51-4836
E-mail: Fabrice.Thomas@ujf-grenoble.fr

[b] Dr. M. Orio
Laboratoire de Spectrochimie Infrarouge et Raman
Bâtiment C5 - UMR CNRS 8516
Université des Sciences et Technologies de Lille
59655 Villeneuve d'Ascq Cedex (France)

Supporting information for this article is available on the WWW under <http://dx.doi.org/10.1002/chem.201303228>.



Scheme 1. Persistent aminyl radical complexes; D and E were isolated as single crystals. The spin density is indicated when available (based on theoretical calculations).^[11,16–20]

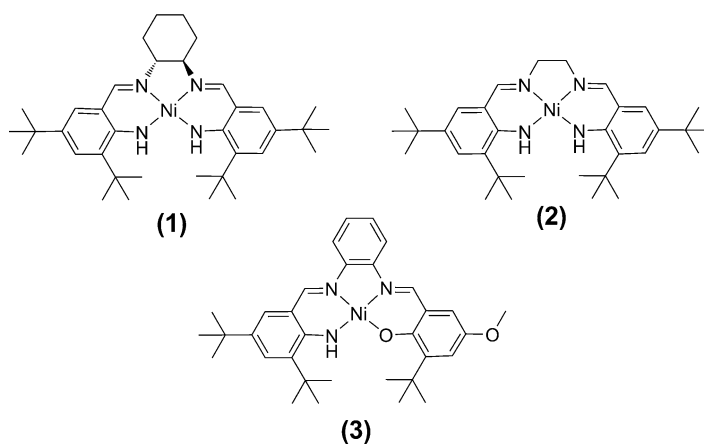
or iridium cation, and resides into a cyclic π -conjugated tropene framework, whereas in Warren's complex it is coordinated to a nickel center and shielded by an adamantane moiety. In both complexes, significant conformational constraints imposed by the ligand contribute to the remarkable stability of the radical species. Notably, significant sharing of the electronic spin is observed between the ligand radical and the metal ion, which bears about 30% of the total spin density. More recently, Betley et al. reported the structural characterization of a high-spin iron(II) complex featuring the terminal imido radical ligand $N(p\text{-}t\text{BuC}_6\text{H}_4)$.^[21] This complex was found to be prone to deliver the nitrene moiety to C–H bond substrates. Apart from these studies, which deal with deprotonated $R_1N^+R_2$ and RN^+ ligands, no structural characterization has been yet reported for coordinated PhNH^+ anilinyll radicals. To the best of our knowledge only one X-ray crystal structure of anilinyll radical has been recently published, and it concerns the tri-*tert*-butylanilinyll free-radical cation.^[22] Surprisingly, the structural features observed experimentally did not coincide with those predicted by calculations some years ago, especially the C–N bond, which is much longer than expected.^[23] This raises an important question that is the influence of the environment on the geometric and subsequently the electronic structures of these radicals.

N_4 -anilinosalens comprise two aminobenzylideneimino moieties connected together through an aliphatic bridge (Scheme 2).^[24–25] Although they have been described in the early 1960s, there are only a few reports with available electrochemical data for metal complexes involving ligands of this family.^[25–26] Higson and McKenzie showed in 1972 that Ni^{II} N_4 -anilidosalens complexes exhibit anodic redox waves in their cyclic voltammetry (CV) curves. They did not draw firm conclusions about the nature of the redox waves in the case of nickel(II) complexes, but clearly established in cobalt(II) complexes that the oxidation process involves "a

change more of metal than ligand oxidation state". Unfortunately, their attempts to isolate any one-electron oxidized complex failed, leading to amorphous solids, which could not be characterized.^[25] Very recently, square-planar copper(II) N_4 -anilinosalen and nickel(II) bis(aminobenzylideneimino) complexes were described, and metal-centered oxidation processes were proposed to account for their electrochemical behavior.^[26] On the other hand, we^[27–28] and others^[29–31] established in a series of papers that the one-electron oxidation of square-planar Ni^{II} salen species (involving phenolate rather than

anilidomoiety) and related complexes was necessarily ligand-centered in non-coordinating solvents, affording phenoxyl radicals that could be, in some cases, isolated. Following this reasoning, N_4 -anilinosalen ligands that are specifically designed to impose a square-planar geometry to a divalent metal ion may be the precursors of stable, and eventually isolable, anilinyll radicals.

We have prepared the nickel(II) complexes **1**, **2**, and **3** from bulky N_4 -anilinosalen ligands (Scheme 2). Whereas **1** and **2** are symmetrical and contain two aniline moieties, complex **3** exhibits a single anilino group. By combining spectro-electrochemistry, UV/Vis/NIR spectroscopy, EPR, and DFT calculations, we herein unequivocally establish for the first time that the Ni^{II} -anilidosalen complexes support a ligand-centered oxidative activity. The corresponding anilinyll radicals $[\mathbf{1}]^+\cdot[\text{SbF}_6]^-$, $[\mathbf{2}]^+\cdot[\text{SbF}_6]^-$, and $[\mathbf{3}]^+\cdot[\text{SbF}_6]^-$, were exceptionally stable and were isolated as single crystals. Despite the fact that $[\mathbf{1}]^+\cdot[\text{SbF}_6]^-$, $[\mathbf{2}]^+\cdot[\text{SbF}_6]^-$, and $[\mathbf{3}]^+\cdot[\text{SbF}_6]^-$ all exhibit an anilinyll radical character, X-ray



Scheme 2. Neutral metal complexes.

diffraction data reveal differences in metric parameters and electronic structure. The anilinyll radical in $[1]^+ \cdot [\text{SbF}_6]^-$ and $[2]^+ \cdot [\text{SbF}_6]^-$ is fully delocalized, thus changes in bond length resulting from oxidation are diluted within the ligand framework. In $[3]^+ \cdot [\text{SbF}_6]^-$ the radical is mainly localized on the anilinyll moiety, allowing a detailed analysis of the structural rearrangement resulting from oxidation. It is significant that neither the expected,^[23] nor the previously reported^[22] geometrical rearrangement resulting from oxidation of anilines account for the present results.

Results and Discussion

Synthesis of the ligands and complexes: The 2-amino-3,5-di-*tert*-butylbenzaldehyde is the key intermediate for the preparation of each ligand. In a reported procedure,^[32] the compound was isolated almost quantitatively after the selective catalytic hydrogenation of 3,5-di-*tert*-butyl-2-nitrobenzaldehyde. However, we failed to reproduce the synthetic method: only mixtures of the desired product together with the fully reduced 4,6-di-*tert*-butyl-2-(hydroxymethyl)aniline were obtained, the latter compound being the major product. In another approach we optimized catalytic hydrogenation to allow quantitative isolation of the 4,6-di-*tert*-butyl-2-(hydroxymethyl)aniline. The compound (air-sensitive) was immediately oxidized with MnO_2 to give the targeted 2-amino-3,5-di-*tert*-butylbenzaldehyde in 92% yield.

The ligands $\text{H}_2\text{L1}$ and $\text{H}_2\text{L2}$ were synthesized by condensation of (*R,R*)-*N,N'*-cyclohexane-1,2-diamine or 1,2-ethylenediamine, respectively, in the presence of two equivalents of 2-amino-3,5-di-*tert*-butylbenzaldehyde. Metalation of $\text{H}_2\text{L1}$ and $\text{H}_2\text{L2}$ with $[\text{Ni}(\text{OAc})_2] \cdot 4\text{H}_2\text{O}$ in the presence of an excess of NEt_3 affords **1** and **2**. The nickel complex **3** was prepared by treating *N*-(3-*tert*-butyl-5-methoxysalicylidene)-phenylene-1,2-diamine with 2-amino-3,5-di-*tert*-butylbenzaldehyde in the presence of a stoichiometric amount of $[\text{Ni}(\text{OAc})_2] \cdot 4\text{H}_2\text{O}$ and two equivalents of NEt_3 . Interestingly, NMR spectroscopy was inappropriate to characterize complexes **1** and **2** at 25 °C. EPR spectroscopy indeed confirmed the presence of about 5% of the paramagnetic species $[1]^+$ and $[2]^+$, resulting from spontaneous air oxidation. Quantitative one-electron oxidation of **1**, **2**, or **3** was performed by the addition of an equimolar amount of $[\text{AgSbF}_6]$ in the non-coordinating solvent CH_2Cl_2 , affording the paramagnetic species $[1]^+ \cdot [\text{SbF}_6]^-$, $[2]^+ \cdot [\text{SbF}_6]^-$, and $[3]^+ \cdot [\text{SbF}_6]^-$.

Characterization of the neutral complexes: The ESI mass spectra of complexes **1–3** display a $[M+H]^+$ molecular ion peak consistent with a metal/ligand ratio of 1:1. Consistent with the symmetry of compounds **1** and **2** the IR spectra exhibit a unique $\nu_{(\text{N-H})}$ vibration band in the 3420–3440 cm^{-1} region. Single crystals of **2** and **3** were grown by slow evaporation of concentrated $\text{MeOH}/\text{CH}_2\text{Cl}_2$ solutions. The structures of **2** and **3** are depicted in Figure 1, whereas Table 1 summarizes the selected bond lengths and angles.

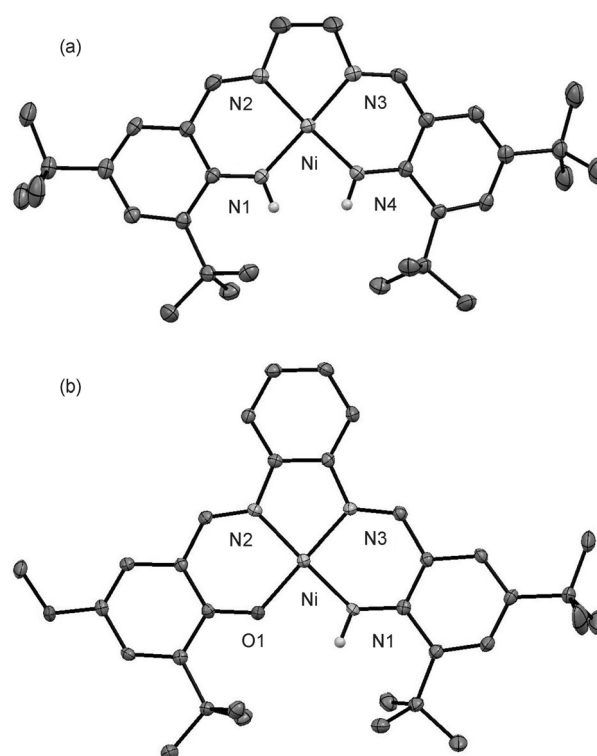


Figure 1. X-ray structures of (a) **2** and (b) **3** at the 30% ellipsoid probability. H atoms omitted for clarity, except the anilido ones.

Table 1. Coordination bond lengths.^[a]

Complexes	Ni–N1	Ni–N2	Ni–N3	Ni–N4	Ni–O1
1	[1.858]	[1.860]	[1.859]	[1.858]	–
2	1.845(4)	1.847(4)	1.835(4)	1.840(3)	–
	[1.857]	[1.854]	[1.853]	[1.857]	
3	1.835(3)	1.836(3)	1.857(3)	–	1.836(2)
	[1.844]	[1.848]	[1.862]		[1.846]
$[1]^+$	1.832(4)	1.865(4)	1.865(5)	1.836(5)	–
	[1.829]	[1.855]	[1.852]	[1.828]	
$[2]^+$	1.820(2)	1.850(2)	1.848(2)	1.830(2)	–
	[1.829]	[1.849]	[1.848]	[1.830]	
$[3]^+$	1.822(4)	1.855(3)	1.843(3)	–	1.836(2)
	[1.825]	[1.851]	[1.850]		[1.822]

[a] Normal text: Experimental bond lengths; Bracket italic: Calculated bond lengths (B3LYP/TZVP) by taking in account solvent effects (see the Experimental Section for details).

In neutral complex **2** the metal ion is coordinated to two imine nitrogen atoms (N2, N3) and two anilido nitrogen atoms (N1, N4). The coordination bond lengths Ni–N1, Ni–N2, Ni–N3 and Ni–N4 are 1.845(4), 1.847(4), 1.835(4) and 1.840(3) Å, respectively. These values are consistent with a diamagnetic low spin configuration of the Ni^{II} ion, as expected for a square-planar nickel complex.^[24f,26b] The extent of tetrahedral distortion could be estimated through the dihedral angle between the opposite N1–M–N2 and N3–M–N4 planes. The measured value is 3°, showing that no significant distortion is present.

In the unsymmetrical complex **3** the metal is coordinated to two imine nitrogens (N2, N3), one anilido nitrogen N1 and one phenolato oxygen (O1), with coordination bond lengths of Ni–N1, Ni–N2, Ni–N3, and Ni–O1 of 1.835(3), 1.836(3), 1.857(3), and 1.836(2) Å, respectively. The dihedral angle between the opposite O1–M–N3 and N1–M–N2 planes is 1°, showing that the metal ion resides within a square-planar geometry, similar to **2**. Interestingly, the distance between the O1 and N1 atoms is 2.510 Å. The O1–H–N1 angle is however 93°, which does not support significant H-bonding interactions between the O1 and N1 atoms.^[33]

Given the absence of crystal structure for **1**, we performed geometry optimizations on this complex. The structures of **2** and **3** were also optimized to provide a benchmark for our calculations. We observed an excellent agreement between the calculated geometries of **2** and **3** and our experimental data (Table 1). As expected, the calculated coordination spheres are similar and symmetrical for both **1** and **2** (Table 1), whereas the metric parameters within the anilido rings are identical in both compounds.

The UV/Vis/NIR spectra of **1**, **2**, and **3** are depicted in Figure 2. They are pretty similar and display two main absorption bands at 27250 cm⁻¹ (6580 M⁻¹ cm⁻¹), 20450 cm⁻¹ (5580 M⁻¹ cm⁻¹) (**1**), and 27200 cm⁻¹ (6650 M⁻¹ cm⁻¹), 20530 cm⁻¹ (4890 M⁻¹ cm⁻¹) (**2**) (Table 2). The highest energy

Table 2. UV/Vis absorption spectra of the complexes.^[a]

Complex	λ_{\max} [cm ⁻¹] (ϵ [L mol ⁻¹ cm ⁻¹])
1	27250 (6580), 20450 (5580)
2	27200 (6650), 20530 (4890)
3	26320 (22870), 22320 sh (10030), 19100 (6930), 16800 sh (4950)
[1]⁺	27174 (5690), 24691 (6300), 21459 (2285), 19646 (1480), 14640 sh (2211), 12437 (7560), 6317 (32 475)
[2]⁺	24752 (7450), 21505 (2950), 18900 (1810), 14620 sh (1820), 12500 (5660), 6493 (24 340)
[3]⁺	27470 (25310), 23590 (10400), 20450 (9320), 15380 sh (2720), 13600 (4040), 6010 (2770)

[a] CH₂Cl₂ solution at 298 K; sh: shoulder, br: broad.

one is assigned to a π - π^* transition involving the amidobenzilideneimino moieties. The lowest energy one was attributed to a charge-transfer transition^[34] (see the Supporting Information and TD-DFT part). The spectrum of **3** is slightly more complex; it is characterized by absorption bands at 26320 cm⁻¹ (22870 M⁻¹ cm⁻¹) and 19100 cm⁻¹ (6930 M⁻¹ cm⁻¹), with shoulders at 22320 cm⁻¹ (10030 M⁻¹ cm⁻¹) and 16800 cm⁻¹ (4950 M⁻¹ cm⁻¹). It is worth noting that the spectrum of **3** is not the sum of the spectra of a Ni^{II}salophen complexes involving 2-*tert*-butyl-4-methoxyphenolate moieties, and **1** or **2**. Thus the anilido and phenolate units are electronically coupled in **3**. It is also of interest that the highest energy band is three times more intense in **3** than in **1** and **2**. This demonstrates that the diamidobenzene moiety contributes significantly to this transition.

Electrochemistry: The electrochemical behavior of complexes **1**, **2**, and **3** has been studied by cyclic voltammetry

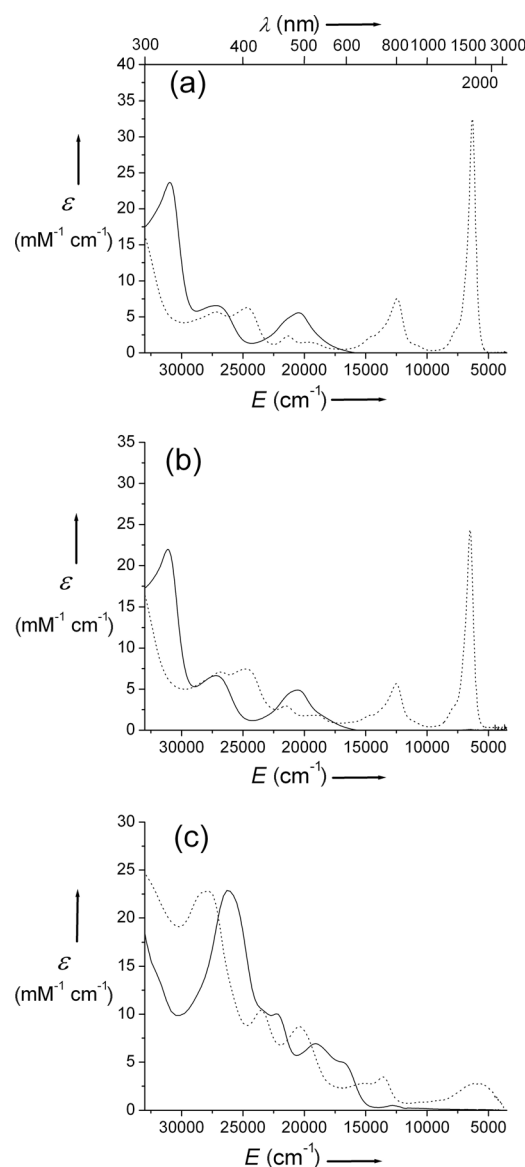


Figure 2. UV/Vis/NIR spectra of (a) **1**, (b) **2**, and (c) **3** and the chemically generated cations a) **[1]⁺**, b) **[2]⁺**, and c) **[3]⁺** in CH₂Cl₂ solution. Black lines: neutral complex, dotted lines: cation. $T = 298$ K.

(CV) in CH₂Cl₂ containing 0.1 M tetra-*n*-butylammonium perchlorate (TBAP) as the supporting electrolyte. Ferrocene was used as standard, and all the potentials are referenced versus the Fc⁺/Fc redox couple. Figure 3 shows the CV curves of **1**, **2**, and **3**. Complexes **1** and **2** exhibit two reversible oxidation waves at $E_{1/2}^1 = -0.30$ V, $E_{1/2}^2 = 0.48$ V, and $E_{1/2}^1 = -0.26$, $E_{1/2}^2 = 0.52$ V vs. Fc⁺/Fc, respectively (Table 3). Both coulometric titration and rotating-disc electrode voltammetry establish that each oxidation process corresponds to a one-electron exchange. Complex **3** exhibits two one-electron oxidation waves, nevertheless only the former system is found to be reversible ($E_{1/2}^1 = 0.10$ V, $E_p^{a,2} = 0.68$ V vs. Fc⁺/Fc). Upon scanning towards the cathodic region of potential (down to about -2.5 V) no reduction wave was evidenced for both **1** and **2**. Thus, these complexes are ex-

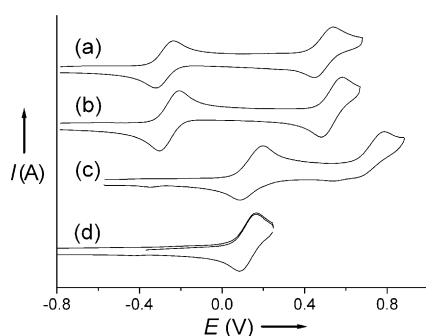


Figure 3. Cyclic voltammograms of (a) **1**, (b) **2** and (c,d) **3** in 0.5 mM CH₂Cl₂ solutions (+0.1 M TBAP). Scan rate: 0.1 V s⁻¹, T = 298 K. The potentials are referenced versus the Fc⁺/Fc couple.

Table 3. Electrochemical properties of the complexes.^[a]

Complex	$E_{1/2}^1$	$E_{1/2}^2$	$\Delta E_{1/2}$
1	-0.30	0.48	0.78
2	-0.26	0.52	0.78
3	0.10	0.68 ^[b]	0.58

[a] In CH₂Cl₂ (+0.1 M TBAP) at 298 K; Reference: Fc⁺/Fc. [b] Irreversible process. The potential corresponds to $E_p^{a,2}$.

tremely robust toward reduction. In contrast, complex **3** displays an irreversible system at $E_p^c = -2.17$ V. Owing to the irreversibility of the wave it is not possible to conclusively assign the redox couple in reduction in this case. We will establish below that the oxidative redox-activity of the complexes is ligand-centered, affording stable anilinyll radicals.

At this stage it is interesting to compare complexes **1**, **2**, and the corresponding salen counterparts.^[27b,29] Firstly, the potential values are cathodically shifted in the N₄-anilinosalens complexes, rendering the oxidized species more accessible. Secondly, the $\Delta E_{1/2}$ value calculated according to $\Delta E_{1/2} = E_{1/2}^2 - E_{1/2}^1$ reflects the extent of electrochemical communication between the redox centers. It is much higher in the N₄-anilinosalen series ($\Delta E_{1/2} = 0.50$ and 0.46 V), leading to the conclusion that anilido nitrogens are more efficient electrochemical couplers than phenolato oxygens. It also points out significant spin delocalization of the radical SOMO in the oxidized species. Complex **3** exhibits the smallest $\Delta E_{1/2}$ value, showing that the radical **[3]⁺** is the most localized within the series. Another informative comparison could be made between the oxidation potentials of **3** and those of symmetrical Ni-salen complexes (involving methoxyphenolate donors) and the Ni^{II} N₄-anilinosalen com-

plexes. $E_{1/2}^1$ neither corresponds to complexes **1** and **2**, nor symmetrical nickel-salen complexes involving methoxyphenolate arms. This again supports an electronic communication between the redox-active rings in the dissymmetric complex **3**, in agreement with UV/Vis data. The $\Delta E_{1/2}$ value is somewhat smaller for **3** than for **1** and **2**, attesting that the communication is weaker in **3**.

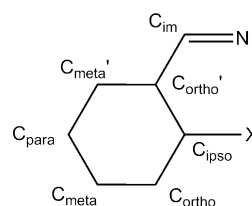
For spectroscopic and structural characterizations of the oxidized products, we generated the cations by either electrolysis or chemical oxidation with silver hexafluoroantimonate (both methods gave similar results). It has to be emphasized that CH₂Cl₂ solutions of the neutral complexes, which are initially brown, turn slowly greenish upon exposure to air (color of the one-electron oxidized species), even in the absence of [AgSbF₆]. The remarkably low $E_{1/2}^1$ values measured for **1** and **2** may explain this behavior. However, the reaction proceeds slowly and was therefore not the most appropriate way to generate the cations quantitatively.

X-ray crystal structures and spectroscopic characterization of one-electron oxidized complexes:

Single crystals of **[1]⁺·[SbF₆]⁻**, **[2]⁺·[SbF₆]⁻**, and **[3]⁺·[SbF₆]⁻** were grown by slow diffusion of pentane into a concentrated CH₂Cl₂ solution. Tables 1, 4, and 5 summarize selected bond lengths and angles for **[1]⁺·[SbF₆]⁻**, **[2]⁺·[SbF₆]⁻**, and **[3]⁺·[SbF₆]⁻**. In all complexes, the nickel ion resides within a square-planar geometry very similar to that of the original neutral complexes. This coordination geometry unequivocally establishes that the nickel ion retains its (+II) oxidation state, the Ni^{III} ion being known to rather exhibit square pyramidal or octahedral geometries. The complexes **[1]⁺·[SbF₆]⁻**, **[2]⁺·[SbF₆]⁻**, and **[3]⁺·[SbF₆]⁻** thus all contain a ligand radical coordinated to a central divalent nickel ion.

The structures of **[1]⁺·[SbF₆]⁻** and **[2]⁺·[SbF₆]⁻** are depicted in Figure 4 and selected bond lengths are listed in Tables 1 and 4. The unit cell of **[2]⁺·[SbF₆]⁻** comprises two

Table 4. Average metric parameters within the amidobenzilideneimino moieties of symmetrical nickel complexes.^[a]



	1	2	[1]⁺	[2]⁺
C _{ipso} -X	[1.349]	1.330(5)/1.340(5) [1.349]	1.335(8)/1.336(7) [1.353]	1.348(3)/1.351(3) [1.352]
C _{ipso} -C _{ortho}	[1.454]	1.441(6)/1.444(6) [1.456]	1.456(8)/1.454(7) [1.449]	1.449(3)/1.447(3) [1.451]
C _{ortho} -C _{meta}	[1.388]	1.366(6)/1.375(6) [1.385]	1.383(8)/1.365(8) [1.388]	1.376(3)/1.381(4) [1.386]
C _{meta} -C _{para}	[1.420]	1.408(6)/1.399(6) [1.423]	1.419(9)/1.430(8) [1.418]	1.423(3)/1.415(4) [1.422]
C _{para} -C _{meta'}	[1.379]	1.354(7)/1.351(6) [1.377]	1.372(9)/1.391(8) [1.384]	1.376(3)/1.372(4) [1.381]
C _{meta'} -C _{ortho'}	[1.415]	1.410(6)/1.403(6) [1.418]	1.379(9)/1.367(8) [1.409]	1.414(3)/1.408(3) [1.411]
C _{ortho'} -C _{ipso}	[1.438]	1.410(6)/1.422(6) [1.438]	1.444(7)/1.452(7) [1.434]	1.430(3)/1.428(3) [1.436]
C _{ortho'} -C _{im}	[1.427]	1.412(6)/1.415(6) [1.424]	1.422(8)/1.437(8) [1.430]	1.432(3)/1.427(4) [1.425]
C _{im} -N	[1.304]	1.288(5)/1.289(6) [1.305]	1.289(7)/1.299(7) [1.301]	1.302(3)/1.298(3) [1.303]

[a] Normal text: Experimental bond lengths (the first and second values correspond to bond lengths within the first and second aromatic ring, respectively); Bracket italic: Calculated bond lengths (B3LYP/TZVP).

Table 5. Metric parameters within the amidobenzilideneimino (X=NH) and phenolato (X=O) moieties for **3** and **[3]⁺**.^[a]

	3 (X=NH)	3 (X=O)	[3]⁺ (X=NH)	[3]⁺ (X=O)
C _{ipso} -X	1.339(4) [1.340]	1.314(4) [1.307]	1.336(5) [1.344]	1.328(5) [1.313]
C _{ipso} -	1.445(4) [1.456]	1.428(4) [1.448]	1.444(6) [1.450]	1.428(6) [1.444]
C _{ortho} -	1.378(4) [1.385]	1.378(4) [1.384]	1.376(6) [1.392]	1.373(6) [1.383]
C _{meta} -	1.413(5) [1.424]	1.409(4) [1.417]	1.394(7) [1.413]	1.400(6) [1.417]
C _{para} -	1.351(4) [1.375]	1.347(4) [1.373]	1.383(7) [1.392]	1.358(6) [1.380]
C _{meta'} -	1.428(4) [1.421]	1.427(4) [1.426]	1.393(6) [1.401]	1.423(6) [1.418]
C _{ortho'} -	1.425(4) [1.445]	1.413(4) [1.431]	1.431(6) [1.441]	1.408(6) [1.431]
C _{ipso} -C _{im}	1.408(4) [1.410]	1.410(4) [1.417]	1.432(6) [1.427]	1.414(6) [1.420]
C _{im} -N	1.321(4) [1.321]	1.313(4) [1.312]	1.290(5) [1.306]	1.306(5) [1.311]

[a] Calculated values are given in bracket italics (B3LYP/TZVP).

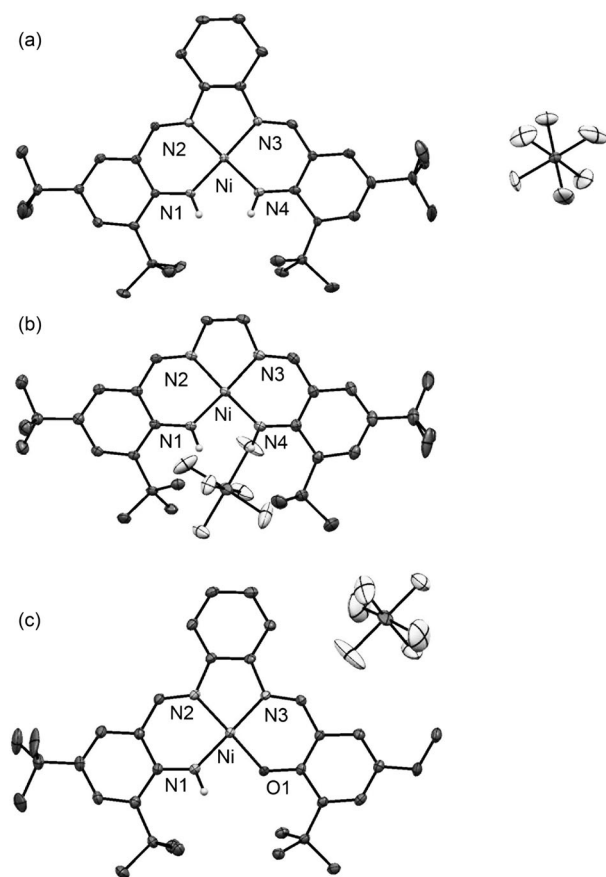


Figure 4. X-ray crystal structures of (a) **[1]⁺·[SbF₆]⁻**, (b) **[2]⁺·[SbF₆]⁻**, (c) **[3]⁺·[SbF₆]⁻**, shown with 30% thermal ellipsoids. The H atoms are omitted for clarity, except the NH ones.

distinct molecules. The metrical parameters do not differ significantly from one molecule to another, thus only one, arbitrary chosen, will be described.

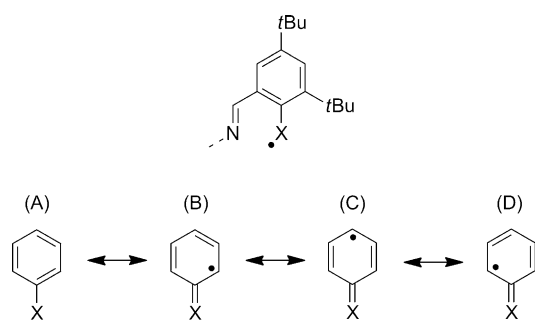
The coordination bond lengths Ni–N1, Ni–N2, Ni–N3, Ni–N4 are 1.832(4), 1.865(4), 1.865(5), and 1.836(5) Å in **[1]⁺**, and 1.820(2), 1.850(2), 1.848(2) and 1.830(2) Å in **[2]⁺**. The almost symmetrical coordination sphere in **[1]⁺·[SbF₆]⁻** and **[2]⁺·[SbF₆]⁻** is clear-cut evidence that the radical is delocalized over the whole ligand framework, a fact confirmed by NIR spectroscopy (see below). The coordination bond distances are very similar when **[1]⁺·[SbF₆]⁻** is compared to **[2]⁺·[SbF₆]⁻**. Thus, the electronic structure of both complexes is identical. By comparing **[2]⁺·[SbF₆]⁻** and **2** it is clear that the Ni–N2 and Ni–N3 distances (Ni–N_{imino}) are essentially unaffected by oxidation, whereas the Ni–N1 and Ni–N4 ones (Ni–N_{anilido}) are shorter by 0.015–0.02 Å in the cation. This global contraction of the coordination sphere is related to the removal of an electron from an antibonding M–L orbital.^[29b,36]

It is now instructive to compare the metrical parameters within the ligand in **[1]⁺** (or **[2]⁺**) with those of the neutral precursor **2**. The individual C_{ipso}–N distances are 1.330(5) Å and 1.339(5) Å in **2**, whereas they are 1.335(8) and 1.336(8) Å in **[1]⁺** and 1.348(3) and 1.351(3) Å in **[2]⁺**, therefore, very similar. Further examination of the C–C distances within the aromatic rings (Table 4) confirms that there is no significant quinoid redistribution of bond lengths upon oxidation. Full delocalization of the radical over the ligand scaffold likely attenuates change in bond lengths upon oxidation. Thus, the present data establishes that **[1]⁺** and **[2]⁺** are constituted of a highly delocalized aniliny radical coordinated to a divalent nickel ion.

The structure of **[3]⁺·[SbF₆]⁻** displays a metal ion located at the center of the mean plane formed by the N1,N2,N3, and O1 atoms (Figure 4c). The O1 and N1 atoms are slightly closer one to the other (2.485(5) Å), as compared with **3**, but the O1–H–N1 angle (93°) is still inconsistent with a strong H-bonding interaction. The coordination bond lengths Ni–N1, Ni–N2, Ni–N3, and Ni–O1 are 1.822(4), 1.855(3), 1.843(3), and 1.836(2) Å in **[3]⁺**, respectively. Within experimental error, complexes **3** and **[3]⁺** thus exhibit similar coordination bond lengths. An interesting structural comparison could be made between the aromatic parts of **3** and **[3]⁺**. Methoxyphenoxy radicals are expected to exhibit shorter C–O and C_{ortho}–C_{meta} bonds, as compared with methoxyphenolates.^[25f,26] However, we do not observe a significant change in metrical parameters for the methoxyphenolate ring on going from **3** to **[3]⁺**. It is the amidobenzilideneimino moiety that displays the most salient structural changes upon oxidation. The imino bond length increases by 0.03 Å, similar to the C_{meta}–C_{para} bond length, whereas the C_{meta}–C_{ortho'} bond length decreases by 0.04 Å. This reveals a fairly localized aniliny radical character of **[3]⁺**, in stark contrast with the delocalized systems observed for **[1]⁺** and **[2]⁺**.

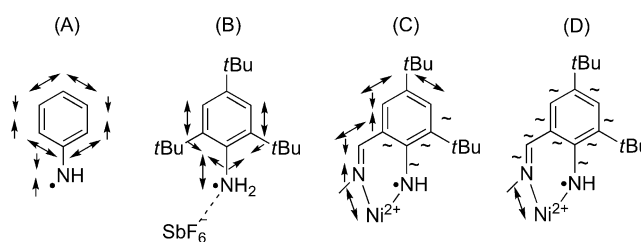
As recently underlined by Shimazaki et al.^[37] radical localization in salen complexes often results in a positioning of the counterion above or at least close to the phenoxy ring. Surprisingly, the crystal structure of **[3]⁺·[SbF₆]⁻** shows an Sb atom that is almost in-plane with the phenolate ring.

Careful examination of the crystal packing of $[3]^+$ $[\text{SbF}_6]^-$ reveals an interesting feature that may explain this surprising behavior. The projection of the crystal structure along the c axis shows that the molecules of $[3]^+$ are arranged in two columns with an almost head-to-tail positioning (see the Supporting Information). Two fluorine atoms of a single $[\text{SbF}_6]^-$ counterion are in weak contact with the anilinyll ring of two molecules of $[3]^+$ belonging to the same column (distances of 4.16 and 4.06 Å between the centroid of the anilinyll rings and the closest F atom). This arrangement is observed two-times per anilinyll moiety, but only on a single side of the ring. Although such interactions are weak, they may contribute to the stability of the localized radical species. Thus, this structural determination unambiguously indicates that $[3]^+$ comprises both a phenolate and an anilinyll radical moiety coordinated to a diamagnetic square-planar divalent nickel ion. In addition, the $\text{C}_{\text{ipso}}-\text{N}$ and $\text{C}_{\text{ortho}}-\text{C}_{\text{meta}}$ bonds remain essentially unaffected by one-electron oxidation. The quinoid distortion is therefore less marked in coordinated anilinyll than in isoelectronic phenoxy radicals.^[27f,28] We interpreted these structural data by an increased weight of canonical structures A and B (Scheme 3) in the case of anilinyll radicals.



Scheme 3. Canonical structures of anilinyll ($\text{X}=\text{NH}$) and phenoxy ($\text{X}=\text{O}$) radicals.

It was initially believed that one-electron oxidation of anilines into anilinyll radicals was accompanied by a quinoid rearrangement of bond lengths.^[23] The shortening of the $\text{C}-\text{N}$ bond in free anilines was, for instance, estimated by DFT calculations^[23] to be about -0.08 Å, thus significantly higher than that experimentally observed here. On the other hand, the first crystal structure of an anilinyll radical (tri-*tert*-butylanilinyll radical) was published recently,^[22] and the authors reported an enlargement of approximately $+0.09$ Å of the $\text{C}-\text{N}$ bond upon one-electron oxidation, instead of a shortening, in sharp contrast with the above DFT investigations. The severe elongation in the crystal structure of the tri-*tert*-butylanilinyll radical was proposed to arise from electrostatic interactions with the counterion, which weakens the $\text{N}_{\text{lonpair}} \rightarrow \pi_{\text{aromatic}}^*$ negative hyperconjugation. We describe here two unprecedented bonding rearrangements that apply to coordinated anilinyll radicals. It is remarkable that anilinyll radicals exhibit such versatility in geometrical structures. It



Scheme 4. Geometrical rearrangements resulting from one-electron oxidation of anilines into anilinyll radicals. A: free anilinyll, calculated without a counterion;^[21] B: tri-*tert*-butyl anilinyll, from the X-ray crystal structure at 123 K;^[20] C: localized ($[1]^+$) and D: delocalized coordinated anilinylls ($[1]^+$ and $[2]^+$) in this work.

is likely that the neighboring environment of the nitrogen plays a crucial role in dictating the bonding rearrangement of anilines upon oxidation (Scheme 4).

Electronic and EPR spectra of anilinyll radical complexes:

The electronic absorption spectra of $[1]^+$, $[2]^+$, and $[3]^+$ in a solution of CH_2Cl_2 are presented in Figure 2.

Radical complexes $[1]^+$ and $[2]^+$ exhibit a characteristic intense band at about 6400 cm^{-1} (1600 nm), whose intensity exceeds $20000\text{ M}^{-1}\text{ cm}^{-1}$ (Table 2 and 6). Given its high intensity and the absence of band above 600 nm in the spectra of the neutral complexes, it is assigned to an intervalence charge-transfer (IVCT) transition. Correspondingly, the experimental line width, about 700 cm^{-1} , is much smaller than the calculated one by using the Hush Equation (3800 cm^{-1}).

$$\Delta\nu_{1/2} = \sqrt{16 \ln 2 RT v_{\text{max}}}$$

Thus, $[1]^+$ and $[2]^+$ are fully delocalized class III compounds according to the Robin Day classification. More details about the assignment of the NIR band are given by TD-DFT calculations (see below; Figure 7). In addition to this strong NIR band, Complexes $[1]^+$ and $[2]^+$ show a moderately intense transition at about 12000 cm^{-1} (ϵ values around $7000\text{ M}^{-1}\text{ cm}^{-1}$, Table 2), together with weaker transitions at about 21000 and 18000 cm^{-1} (Table 2), which are attributed to charge-transfer (CT) transitions. An additional prominent transition is observed at a slightly higher energy (ca. 24000 cm^{-1}), which is very similar to the prototypical band of free anilinyll radicals.^[38]

Complex $[3]^+$ exhibits a NIR band at 6010 cm^{-1} , which is assigned to an IVCT transition (Table 6). It is very interest-

Table 6. NIR band shape analysis of the one-electron oxidized complexes.^[a]

Complex	$\tilde{\nu}_{\text{max}}$ [cm^{-1}]		ϵ [$\text{L mol}^{-1}\text{ cm}^{-1}$]	$\Delta\tilde{\nu}_{1/2}$
	Exptl	Calcd		
$[1]^+$	6317	6832	32 475	670
$[2]^+$	6493	7273	24 340	740
$[3]^+$	6010	5934	2770	3720

[a] Chemically generated cations; CH_2Cl_2 solution at 298 K.

ing that its intensity is much lower for $[3]^+$ ($2770\text{ M}^{-1}\text{ cm}^{-1}$) than for $[1]^+$ and $[2]^+$. Because the intensity is correlated with the degree of localization in mixed-valence compounds, it is clear that $[3]^+$ is the most localized radical in the series. Thus, unlike symmetrical compounds, complex $[3]^+$ does not belong to a class III-, but rather to a class II mixed-valence compound, in perfect agreement with the solid-state structure. Additional features are observed in the UV/Vis region at $13\,600$, $20\,450$ and $23\,590\text{ cm}^{-1}$.

The EPR spectra of $[1]^+\cdot[\text{SbF}_6]^-$, $[2]^+\cdot[\text{SbF}_6]^-$, and $[3]^+\cdot[\text{SbF}_6]^-$ have been recorded in frozen CH_2Cl_2 solution at 100 K . All complexes are paramagnetic ($S=1/2$). In neat CH_2Cl_2 the signal is mainly isotropic and centered at g values within the range 2.018 – 2.024 . This is the hallmark of a mainly ligand-centered singly occupied molecular orbital (SOMO).^[27–31] In the presence of 10% pyridine the anisotropy could be resolved, revealing identical spectra for $[1]^+$ and $[2]^+$ (Figure 5). A rhombic pattern is observed, without

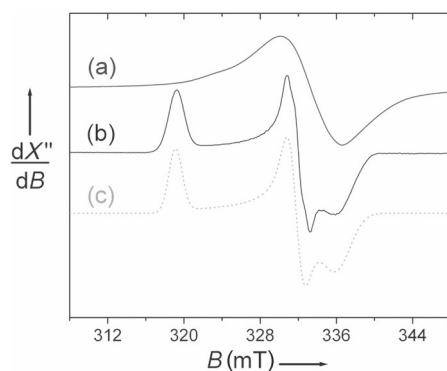


Figure 5. EPR spectra of $[1]^+$ in (a) CH_2Cl_2 and (b) in $\text{CH}_2\text{Cl}_2 + 10\%$ pyridine ($c=0.5\text{ mm}$); (c) simulation using the parameters given in the text. Microwave freq.= 9.42 GHz , power= 8 mW , mod. freq. 100 KHz , amp. 0.3 mT , $T=100\text{ K}$.

any clearly distinguishable hyperfine splitting with ^{14}N nuclei. From simulation the following g -values were obtained: $g_1=2.091$, $g_2=2.011$, $g_3=1.985$ ($g_{\text{av}}=2.029$). We would like first to comment on this g -anisotropy. The three-coordinate β -ketimidate $[(\text{Me}_3\text{NN})\text{Ni}=\text{NAd}]$ complex (Figure 1) reported by Warren et al.^[19] (the only Ni^{II} -aminyl radical complex published so far from which both structural and EPR data are available) exhibits a much larger g -anisotropy, with $g_1=2.162$, $g_2=2.038$, $g_3=1.937$ ($g_{\text{av}}=2.046$). This is indicative of a substantial contribution of the nickel $3d$ -orbitals to the SOMO. As underlined by the authors, this sharing results from an optimal overlap between the N-centered p_x -orbital of the linear coordinated aminyl radical and the in-plane half-occupied d_{xy} metal orbital (tricoordinated metal ion). DFT calculations correspondingly reveal that only 57% of the total spin density is harbored by the nitrogen atom. The bonding scheme is clearly different in $[1]^+$ and $[2]^+$ since the nickel ion lies within a square-planar geometry. In these cases the overlap between the nickel and π -radical orbital is weaker (it involves an out-of-plane d_{yz}

metal orbital), resulting in a smaller g -anisotropy and a more conspicuous aniliny radical character of the complexes. On the other hand, given the rich literature data on octahedral Ni^{III} complexes formed by oxidation of square-planar Ni^{II} -radical salen complexes in coordinating solvents,^[39] it is remarkable that the average g value remains similar both in presence and absence of pyridine. The square-planar Ni^{II} -aniliny radical complex is therefore not converted into a square-pyramidal or octahedral Ni^{III} -anilido complex even in the presence of 10% of a strong donor. This is strong evidence that the ligand field provided by the aniliny donors is stronger than that of phenoxy radicals.^[40]

The g_{iso} value is slightly smaller in $[3]^+$ than in $[1]^+$ and $[2]^+$, when the spectrum is recorded in CH_2Cl_2 . Thus, the metallic contribution to the SOMO is substantially smaller in the localized aniliny radical $[3]^+$. On the other hand, the spectrum of $[3]^+$ is significantly different than those of $[1]^+$ and $[2]^+$ when it is recorded in the $\text{CH}_2\text{Cl}_2/\text{pyridine}$ ($90:10$) mixture, with signals at $g_1=2.230$, $g_2=2.158$, $g_3=2.026$ ($g_{\text{av}}=2.138$, see the Supporting Information). These values are consistent with a Ni^{III} -anilido rather than Ni^{II} -aniliny radical character of the complex in this medium. In $[3]^+$, the square-planar nickel(II) ion rearranges into an octahedral Ni^{III} center by axial coordination of two pyridine molecules. This fact confirms that aniliny radicals are rather strong donors.

DFT calculations: The structures of both the neutral compounds **1**, **2**, and **3** (see above; Figures S1–S3, the Supporting Information) and the corresponding cations $[1]^+$, $[2]^+$, and $[3]^+$ (Figures S4–S6, the Supporting Information) have been optimized. As shown in Tables 1, 4, and 5 there is a fairly good agreement between the calculated bond lengths and the experimental values. The larger discrepancies (0.02 \AA) are observed for the coordination bond lengths. Such behavior is not surprising and typical of current DFT functionals.^[41] It is significant that the metrical parameters within the organic part of the molecules and especially within the aromatic rings, are very accurately predicted, with errors that do not exceed 0.015 \AA .

Both the bonding scheme and geometrical changes resulting from one-electron oxidation are similar for **1** and **2**. They slightly differ in the case of **3**. We will therefore limit our discussion to **1** and **3** and their corresponding cations.

The most salient structural change resulting from one-electron oxidation in the series is the slight shortening of the $\text{Ni}-\text{N}_{\text{aniliny}}$ bonds, which nicely reproduces the trend observed experimentally. From 1.858 \AA in **1** it decreases to 1.829 \AA in $[1]^+$, whereas from 1.844 \AA in **3** it decreases to 1.825 \AA in $[3]^+$. This shortening is interpreted by an enhanced metal-to-ligand back-donation in the cation,^[29b,37] a fact confirmed by the enhanced Mulliken charge density at the metal nucleus, 0.5964 for **1** versus 0.7412 for $[1]^+$ and 0.6716 for **3** versus 0.7959 for $[3]^+$.

Because discrepancies were reported in literature regarding the bonding scheme of aniliny radicals (especially the change in C–N bond length)^[22,23] it is particularly important

to comment the predicted rearrangements of bond lengths upon oxidation. Firstly, the predicted bonding changes within the ligand upon one-electron oxidation do not exceed 0.006 Å in the symmetrical compound $[1]^+$, and mainly concern the anilido moieties. Full delocalization of the SOMO over both aromatic rings here "dilutes" the structural changes within the organic framework. This assumption can be verified by examination of the predicted bonding changes resulting for one-electron oxidation of **3** into $[3]^+$. The magnitude of the change in bond lengths is indeed higher: The main changes in bond lengths concern the $C_{\text{meta}}-C_{\text{para}}$, $C_{\text{para}}-C_{\text{meta}}$ and $C_{\text{meta}}-C_{\text{ortho}}$ bonds, as observed experimentally (the numbering is shown in Table 4). The calculated changes are -0.011 , $+0.017$, and -0.020 Å, respectively. Remarkably, the $C_{\text{ipso}}-N$ bond length is essentially unaffected by oxidation as the predicted change does not exceed 0.004 Å. Thus, oxidation of **3** into $[3]^+$ induces only a moderate quinoid redistribution of bond lengths, without significant change in the $C_{\text{ipso}}-N$ bond length.

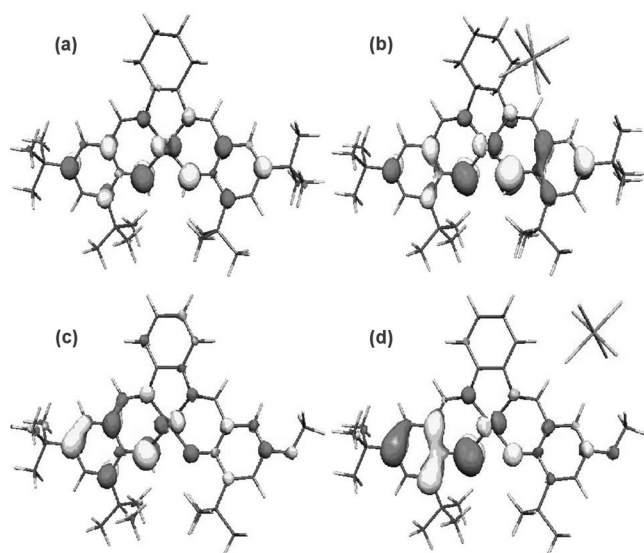


Figure 6. Higher occupied orbitals of (a) **1** (HOMO), (b) $[1]^+\cdot[SbF_6]^-$ (SOMO), (c) **3** (HOMO) and (d) $[3]^+\cdot[SbF_6]^-$ (SOMO).

The HOMO of neutral **1** represents the antibonding combination of the Ni $3d_{yz}$ and an out-of-plane ligand π orbital, with contributions of 20 and 80 %, respectively (Figure 6). The π -orbital is delocalized and equally developed on both anilido rings. One-electron oxidation creates a hole in the HOMO of **1**, which becomes the SOMO in $[1]^+$. Thus the SOMO of $[1]^+$ is basically the centrosymmetric combination of the SOMO of two coordinated "half" anilinyll radicals. As for **1**, the HOMO of **3** is an antibonding combination of the Ni $3d_{yz}$ and delocalized ligand π orbitals, with contributions of 14 and 86 %, respectively. It is worth noting that the contributions of the aromatic fragments are not equivalent: The central phenyl group accounts for 10 %, the anilido moiety

(including the imino group) accounts for 55 % and the phenolato group (including the imino group) accounts for 20 % of the HOMO. The SOMO of $[3]^+$ exhibits features similar to the HOMO of **3**, with somewhat slightly different contributions of the organic fragments, due to relaxation. For instance, the central phenyl group does not contribute significantly to the SOMO, whereas the anilido moiety now accounts for 65 %.

Let us first comment on the shape of the ligand-centered SOMOs. Adamo et al. previously investigated benzyl and phenoxy radicals and qualitatively analyzed the SOMO in terms of interactions between the singly occupied atomic orbital of the exocyclic group X and the matching π -orbitals of the benzene ring.^[42] For benzyl radicals ($X=CH_2$) the exocyclic group interacts equally with the π and π^* orbitals of the benzene moiety. As a consequence of the X group, C_{ortho} and C_{para} atoms contribute significantly to the SOMO. When the methylene group is replaced by an oxygen atom (phenoxy radicals), the singly occupied atomic orbital of X is lower-lying. The singly occupied atomic orbital of the oxygen then interacts much strongly with the benzene π -orbital, with two important consequences: The contribution of the benzene π orbital to the SOMO increases, whereas that of the X group decreases. In anilinyll radicals an intermediate situation is encountered: The electronegativity of the nitrogen atom is indeed intermediate between those of C and O. Thus, the SOMO is more developed on the heteroatom and less on the benzene ring comparatively to isoelectronic phenoxy radicals. As a consequence the quinoid distribution of bond lengths is less perceptible in anilinyll than in phenoxy radicals, as observed experimentally.

Another important outcome of the analysis of the ligand-centered SOMOs concerns its relative distribution over the aromatic rings. It is equally shared between both peripheral rings in $[1]^+$ and $[2]^+$ (mixed-valence compound), in agreement with Vis/NIR data. In the case of $[3]^+$ the SOMO is 65 % localized on the anilido and 20 % localized on the phenolato moiety. As expected, the diaminobenzene ring does not contribute significantly to the SOMO. These results, consistent with Vis/NIR data, confirm that $[3]^+$ behaves like a class II mixed-valence species.

If we now focus on the entire complex and not solely the organic part of the ligand, it is clear that the SOMOs of $[1]^+$, $[2]^+$, and $[3]^+$ are essentially ligand-centered, but they readily mix with the out-of-plane Ni $3d_{yz}$ orbital. Thus, they acquire a metal character of 21, 20, and 15 % for $[1]^+$, $[2]^+$, and $[3]^+$, respectively. One can anticipate a significant orbital angular momentum and subsequent large g shifts in the EPR signature of the compounds. Accordingly, the calculated principal values for the g -tensor are exceedingly anisotropic for pure organic radicals: $g_1=2.072$, $g_2=2.015$, $g_3=1.986$; $g_1=2.067$, $g_2=2.014$, $g_3=1.983$; $g_1=1.983$, $g_2=2.014$, $g_3=1.995$ for $[1]^+$, $[2]^+$, and $[3]^+$, respectively (in which the lowest g component points orthogonal to the anilinyll plane, and the medium one along the C–N bond). These values compare fairly with the experimental ones (Table 7). In addition, the calculated g_{iso} values of about 2.02 are in excel-

Table 7. EPR parameters of the aniliny radical complexes.^[a]

Complex	EPR properties
[1] ⁺	<i>g</i> _{iso} = 2.024 (CH ₂ Cl ₂) <i>g</i> ₁ = 2.091, <i>g</i> ₂ = 2.011, <i>g</i> ₃ = 1.985 (CH ₂ Cl ₂ + pyridine) <i>[g</i> ₁ = 2.072, <i>g</i> ₂ = 2.015, <i>g</i> ₃ = 1.986 (<i>g</i> _{iso} = 2.024)]
[2] ⁺	<i>g</i> _{iso} = 2.024 (CH ₂ Cl ₂) <i>g</i> ₁ = 2.091, <i>g</i> ₂ = 2.011, <i>g</i> ₃ = 1.985 (CH ₂ Cl ₂ + pyridine) <i>[g</i> ₁ = 2.067, <i>g</i> ₂ = 2.014, <i>g</i> ₃ = 1.983 (<i>g</i> _{iso} = 2.021)]
[3] ⁺	<i>g</i> _{iso} = 2.018 (CH ₂ Cl ₂) <i>g</i> ₁ = 2.230, <i>g</i> ₂ = 2.158, <i>g</i> ₃ = 2.026 (CH ₂ Cl ₂ + pyridine) <i>[g</i> ₁ = 2.056, <i>g</i> ₂ = 2.014, <i>g</i> ₃ = 1.995 (<i>g</i> _{iso} = 2.021)]

[a] Calculated values are given in italics in brackets.

lent agreement with the fact that the unpaired electron resides mainly, but not exclusively, in a π* orbital.

Consistent with the molecular orbital analysis, and as expected for odd-alternant cyclic π-radicals, positive spin populations are found at the aniliny nitrogen, C_{ortho}, C_{para}, and C_{ortho'} atoms for [1]⁺, [2]⁺, and [3]⁺ (Table 8). It is instruc-

Table 8. Mulliken spin populations.

	[1] ⁺	[2] ⁺	[3] ⁺ ^[a]	[3] ⁺ ^[b]
Ni	0.19	0.18	0.13	
X	0.13/0.16	0.14/0.16	0.35	0.07
C _{ipso}	0	0	0	0
C _{ortho}	0.06/0.08	0.07/0.09	0.10	0.02
C _{meta}	0	0	0	0
C _{para}	0.08/0.10	0.09/0.11	0.12	0.02
C _{meta'}	0	0	0	0
C _{ortho'}	0.06/0.08	0.07/0.09	0.08	0.02

[a] anilido part, X = NH (the contribution of the H atom is not included in the Table. [b] phenolato part, X = O.

tive to compare the spin distribution pattern in aniliny radicals (Figure S8, the Supporting Information) with that observed for isoelectronic phenoxyl radicals. We previously reported the electronic structure of a square-planar Ni^{II} salen radical complex involving a localized di-*tert*-butylphenoxyl moiety.^[27f] We found that the contribution of the phenoxyl oxygen, C_{ipso}, C_{ortho}, C_{ortho'} and C_{para} carbons were 0.24, 0.10, 0.15, 0.16, and 0.25, respectively.^[27f] In the case of [3]⁺, the individual contributions of the nitrogen, C_{ipso}, C_{ortho}, C_{para} and C_{ortho'} atoms are 0.35, 0.00, 0.10, 0.12, and 0.08, respectively. Thus, the contribution of the C_{ipso} and C_{para} carbons dramatically decreases at the expense of the exocyclic heteroatom in aniliny radicals. These results are in excellent agreement with the notion that the lower electronegativity of the nitrogen atom enhances the weight of the resonance structures A and B (Scheme 3) in aniliny-versus phenoxyl radicals.

TD-DFT calculations: To assign the Vis/NIR transitions we performed TD-DFT calculations on the optimized structures of [1]⁺, [2]⁺, and [3]⁺ (Figure 7)

Before discussing the spectra of the radical complexes we will first focus on the neutral species. Because the nature of the transitions and their energy is quite similar for **1** and **2**,

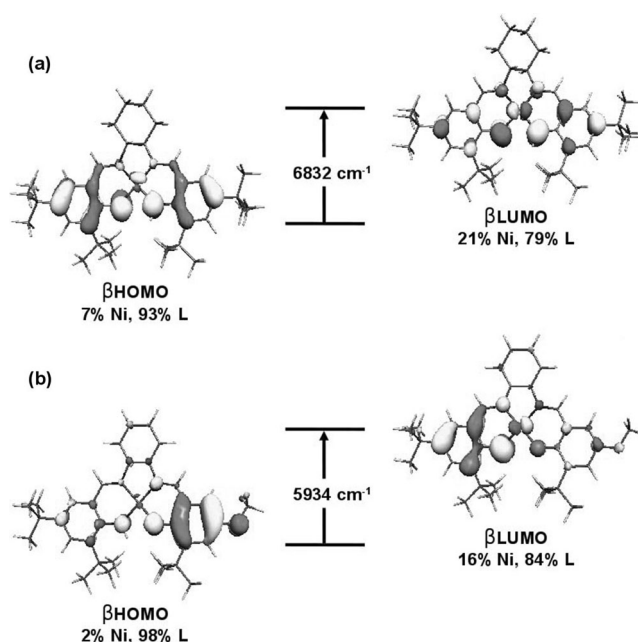


Figure 7. TD-DFT assignment of the lowest energy electronic excitation for (a) [1]⁺ and (b) [3]⁺.

only the results concerning the former will be discussed below. Thus for **1**, two principal electronic excitations are calculated at 22917 and 26292 cm⁻¹, which match quite well the experimental bands at 20450 and 27250 cm⁻¹. They correspond mainly to nickel-to-amidobenzilideneimino CT transitions (Figures S20 and S21). No transition is predicted in the NIR region.

For **3**, the three lowest energy excitations are predicted at 20152, 22685, and 25893 cm⁻¹. They all correspond to the CT transition toward the whole aromatic framework (Figure S22, the Supporting Information). The donor orbitals are either delocalized π-orbitals with substantial metallic character (transitions at 20152 and 25893 cm⁻¹) or purely metal-centered (d_{z²}) in the transition at 22685 cm⁻¹. A good agreement is found between these calculated excitations and the experimentally observed bands at 19100, 22320, and 26320 cm⁻¹.

The experimental electronic spectra of [1]⁺, [2]⁺, and [3]⁺ exhibit a fingerprint in the NIR region at about 6000 cm⁻¹ (Table 6). Accordingly, TD-DFT calculations predict a band at about 6000 cm⁻¹ for the radical complexes [1]⁺–[3]⁺ (Figure 7). In all cases this is the lowest energy excitation and it corresponds to a β-HOMO→β-LUMO transition.

For the cations [1]⁺ and [2]⁺ the calculated energies are 6832 cm⁻¹ (*f* = 0.215) and 7273 cm⁻¹ (*f* = 0.218), respectively. We incorporated the counterion [SbF₆]⁻ in all our calculations on the cations. Nevertheless we found that its influence was only marginal, since in its absence the calculated excitations are shifted by only 20 cm⁻¹. The β-LUMO is mainly an anti-centrosymmetric combination of two equally developed aniliny π-orbitals, with 21% contribution of a metallic d_{yz}

orbital. The β -HOMO is a centrosymmetric combination of two equivalent anilinyll π -orbitals, with small but sizeable metal d_{xz} contribution (7%). Thus, the β -HOMO \rightarrow β -LUMO excitation is assigned to an intervalence (IV) CT transition of a fully delocalized class III compound according to the Robin Day classification.

Interestingly, a higher electronic excitation is calculated at 13698 cm^{-1} ($f=0.100$) and 13227 cm^{-1} ($f=0.100$) for $[1]^+$ and $[2]^+$, respectively. It corresponds to an intraligand CT transition (β -HOMO-2 \rightarrow β -LUMO) in which the donor orbital is a delocalized π -system involving the amidobenzilideneimino rings (Figures S23 and S24).

For $[3]^+$ we calculated two low energy excitations at 5934 cm^{-1} ($f=0.086$) and 13831 cm^{-1} ($f=0.023$) that fairly compare with the experimental bands (6010 and 13600 cm^{-1}). The 5934 cm^{-1} transition corresponds to the β -HOMO \rightarrow β -LUMO transition, involving predominantly ligand-centered orbitals. The donor orbital is a delocalized π -orbital mainly developed on the phenolate ring, whereas the acceptor one is mainly located on the anilinyll ring (with 16% contribution of the metal) and corresponds to the SOMO. Thus it is ascribed to an IVCT transition. Consequently, $[3]^+$ is assigned to a class II mixed valence compound. A higher energy excitation is predicted at 13831 cm^{-1} , which is assigned to a β -HOMO-4 \rightarrow β -LUMO transition (Figure S25, the Supporting Information). The donor orbital is again mainly ligand-centered but the principal contribution comes from the diamidobenzene ring, with a metallic contribution of 2%. It is therefore ascribed to a main intraligand CT transition.

Thus TD DFT calculations support the assignment of $[1]^+$ and $[2]^+$ as class III mixed-valence compounds, and $[3]^+$ as a class II mixed-valence compound.

Discussion and Conclusion

The structures of the isoelectronic phenoxyll, anilinyll, benzyl and phenylthiyl radicals unbound to a metal ion have been established by DFT calculations some years ago.^[16,23,42,43] The main finding was that the phenoxyll and anilinyll radicals exhibit roughly the same behaviour: a quinoid bond pattern was evidenced, with relatively short $C_{\text{ortho}}-C_{\text{meta}}$ and $C_{\text{ipso}}-X$ (in which $X=O$ or NH/NH_2) bonds, and comparatively longer $C_{\text{ipso}}-C_{\text{ortho}}$ and $C_{\text{meta}}-C_{\text{para}}$ bonds. In the case of phenylthiyl radicals, which at a first glance may be also considered as odd-alternant π -radicals, it was noticed that the C-C bonds were almost equivalent. This leads to the important conclusion that the unpaired electron is delocalized over the aromatic ring in phenoxyll and anilinyll radicals, whereas it is rather localized at the sulphur atom in phenylthiyl radicals. The predicted quinoid pattern of bonds was nicely verified experimentally in the crystal structures of the tri-*tert*-butylphenoxyll radical^[44] and one-electron oxidized Ni^{II} - and Cu^{II} -salen complexes, which both contain one coordinated phenoxyll radical.^[28,29,45] Surprisingly, in the first crystallographic investigation on anilinyll radicals (tri-*tert*-butylanilinyll radi-

cal) it was shown that the $C_{\text{ipso}}-X$ bond length was elongated rather than contracted.^[22]

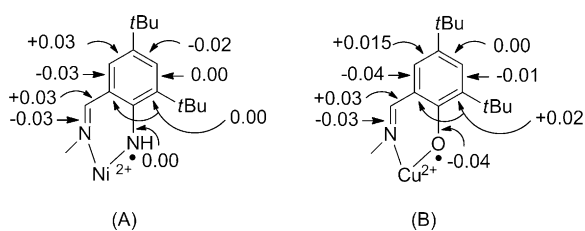
Both $[1]^+$ and $[2]^+$ harbor a coordinated anilinyll radical moiety, but no significant change of bond length was observed within the aromatic ring on going from the bis-(anilido) to the radical compound. This is clear evidence that the expected structural rearrangement after removal of the electron is "diluted" in the aromatic framework. Thus, the anilinyll radical is delocalized over both aromatic rings. Consequently, complexes $[1]^+$ and $[2]^+$ are assigned as class III mixed valence compounds according to the Robin Day classification. Clearly, delocalization of the SOMO in $[1]^+$ and $[2]^+$ occurs through the nickel ion, due to both geometric and energetic matches between the anilinyll π -orbitals and an out-of-plane nickel 3d orbitals. EPR spectroscopy was used to experimentally probe the metallic contribution to the SOMO. The g value deviates significantly from the free electron value (2.0023), in agreement with a non-negligible contribution of the nickel to the SOMO. DFT calculations reproduced the experimental g-values and provided an estimate for the contribution of the nickel 3d_{yz} orbital, which is roughly 20%. This amount, although non-negligible, is much lower than that reported for complexes involving coordinating aminyl described so far.^[11,19-20]

The assignment of $[1]^+$ and $[2]^+$ as fully delocalized class III mixed-valence compounds in solution is supported by NIR spectroscopy. A strong IVCT transition is indeed observed at 6317 (32475), and 6493 cm^{-1} ($24340\text{ M}^{-1}\text{ cm}^{-1}$) for $[1]^+$ and $[2]^+$, respectively.

An interesting comparison could be made between $[1]^+$ and its salen counterpart, which is also a class III mixed valence compound.^[29b] The experimental energetic gap between the β -HOMO and β -LUMO (corresponding to the IVCT transition) is higher for anilinyll compounds, although these two radical complexes exhibit a similar geometry, with almost the same metal contribution to the SOMO. This shift originates from differences in the electronic structure of anilinyll as compared with phenoxyll radicals (see below).

In the unsymmetrical compound **3** the situation differs significantly. Its coordination sphere comprises both phenolate and anilido moieties, whose redox active orbitals lie at different energies. One-electron oxidation therefore occurs preferentially at a single site of the molecule. X-ray diffraction shows that the metrical parameters within the phenolate group are not affected by oxidation of **3** to $[3]^+$. In contrast, the bond lengths within the anilido moiety are significantly altered, with a contraction of one $C_{\text{ortho}}-C_{\text{meta}}$ bond and an elongation of one $C_{\text{meta}}-C_{\text{para}}$ bonds. Thus $[3]^+$ contains a rather localized anilinyll radical moiety. Complex $[3]^+$ exhibits an IVCT transition in the same energy range than $[1]^+$ and $[2]^+$, but its intensity is much lower ($2770\text{ M}^{-1}\text{ cm}^{-1}$). Thus, both the solid-state structure and NIR spectroscopy supports the description of $[3]^+$ as a class II mixed-valence compound.

The structural rearrangements observed upon oxidation of the anilido into anilinyll moiety provide major insights onto the electronic structure of the radical. The most salient



Scheme 5. Experimental structural rearrangements (in Å) resulting from radical formation in localized and coordinated (A) amidobenzilideneimino and (B) salicylidene moieties. (A): Complex **3**; (B): From ref. [45] (for each bond the difference between the phenoxyl and phenolate ring within the same molecule is indicated).

feature is the absence of elongation of the C–X bond, and a globally less marked quinoid bond pattern when anilinyll is compared with isolectronic phenoxyl radicals (Scheme 5). When the oxygen heteroatom of a phenoxyl radical is replaced by a nitrogen atom, the energy of the corresponding singly occupied atomic orbital increases (due to the lower electronegativity of this element).^[42] The interaction of the heteroatom with the benzene π -orbital is consequently altered: The SOMO is more developed on the heteroatom and less on the benzene ring in anilinyll as compared with phenoxyl radicals. Thus the quinoid bond pattern and more specifically the change in C–X bond length are less perceptible in anilinyll than in phenoxyl radicals. This fact could be also evidenced through examination of the Mulliken spin population at the C_{ipso} carbon: it is almost negligible in anilinyll, whereas it is classically 0.10–0.20 in phenoxyl radicals. Another important outcome of the analysis of the Mulliken spin population concerns the spin population at the metal center: It is about 18% for **[1]⁺** and **[2]⁺**, 13% for **[3]⁺**, but it is more than 25% for the very few crystallized M–N_{aminyl} complexes reported so far.^[11,19–20] The contribution of the Mⁿ⁺–N_{aminyl} electronic isomer versus the Mⁿ⁺¹⁺–N_{anilido} one is thus substantially higher for compounds **[1]⁺**, **[2]⁺**, and **[3]⁺**.

The remarkable versatility in the geometric structures of anilinyll radicals has to be underlined. In seminal investigations it was reported that one-electron oxidation of anilines to anilinyll radicals induces a quinoid rearrangement of bond lengths.^[23] For example, the C–N bond was predicted to be shortened by 0.08 Å after oxidation in the case of simple free aniline.^[23] The crystal structure of the tri-*tert*-butylanilinyll radical was solved recently,^[22] and the authors reported a surprising enlargement of 0.09 Å of the C–N bond in the radical as compared to the aniline precursor. Interactions between the counterion ([SbF₆][−], similar to that used in the present study) and the NH₂ group were detected in the structure, and proposed to contribute to the unexpected elongation of the C–N bond. In the present study the anilinyll moieties are deprotonated, coordinated to a metal ion, and do not interact significantly with the [SbF₆][−] counterion. In complexes **[1]⁺**–**[3]⁺** we did not observe any significant change in the C–N bond length, whether the anilinyll is localized or delocalized. Thus metal coordination prevents

non-specific variations (e.g., mainly due to interaction with the counterion) in the C_{ipso}–N_{aminyl} bond length. These results show that the neighbouring environment of the anilinyll nitrogen (no ion,^[23] counterion,^[22] or metal ion) has a major influence on both the geometric and electronic structures of anilines upon oxidation. Further investigations on the reactivity of anilinyll radical complexes are currently underway in our laboratory.

Experimental Section

General: X-Band EPR spectra were recorded on a BRUKER EMX Plus spectrometer controlled with the Xenon software and equipped with a Bruker teslameter. A Bruker nitrogen flow cryostat connected to a high sensitivity resonant cavity was used for 100 K measurements. An Oxford Instrument Helium flow cryostat connected to a dual mode resonant cavity was used to run experiments at 10 K. The spectra were simulated using the SIMFONIA software (BRUKER). NMR spectra were recorded on a Bruker AM 300 (¹H at 300 MHz, ¹³C at 75 MHz) or a Bruker Avance 400 (¹H at 400 MHz, ¹³C at 100 MHz). Chemical shifts are given relative to solvent residual peak. Mass spectra were recorded on a Bruker Esquire 3000 (ESI/Ion Trap) equipment. Microanalysis were performed by the Service Central d'Analyse du CNRS (Lyon, France). 298 K UV/Vis/NIR spectra were recorded on a Perkin–Elmer Lambda 1050 spectrophotometer equipped with a temperature controller unit set at 298 K. The quartz cell path length is 1.000 cm. Cyclic voltammetry curves were recorded on a CHI 620 potentiostat in a standard three-electrode cell under Argon atmosphere. An AgNO₃/Ag (0.01 M) reference electrode was used. All the potential given in the text are referred to the regular Fe⁺/Fe redox couple used as external reference. A vitrous carbon disc electrode (5 mm diameter) polished with 1 mm diamond paste was used as working electrode. Electrolysis was performed on a PAR 273 potentiostat, under Argon atmosphere at −40 °C, using a carbon felt working electrode.

Crystal structure analysis: Collected reflections were corrected for Lorentz and polarization effects but not for absorption in the case of **1** and **[1]⁺**·[SbF₆][−]. For the other structures SADABS-2004/1 was used for absorption correction. The structures were solved by direct methods and refined by using the TEXSAN^[46] and OLEX2 softwares.^[47] All non-hydrogen atoms were refined with anisotropic thermal parameters. Hydrogen atoms were generated in idealized positions, riding on the carrier atoms, with isotropic thermal parameters except the hydroxyl ones, which were localized on the Fourier map and fixed. CCDC-(954385–954389) contain the supplementary crystallographic data for this paper CCDC-954385 (**2**), CCDC-954386 (**3**), CCDC-954387 (**[1]⁺**·[SbF₆][−]), CCDC-954388 (**[2]⁺**·[SbF₆][−]) CCDC-954389 (**[3]⁺**·[SbF₆][−]) contain the supplementary crystallographic data for this paper. These data can be obtained free of charge from The Cambridge Crystallographic Data Centre via www.ccdc.cam.ac.uk/data_request/cif.

Computational details: All theoretical calculations were performed with the ORCA program package.^[48] Full geometry optimizations were carried out for all complexes using the B3LYP hybrid functional^[49–51] in combination with the TZV/P^[52] basis set for all atoms and by taking advantage of the resolution of the identity (RI) approximation in the Split-RI-J variant^[53] with the appropriate Coulomb fitting sets.^[54] Increased integration grids (Grid4 in ORCA convention) and tight SCF convergence criteria were used. Solvent effects were accounted for according to the experimental conditions. For that purpose, we used the CH₂Cl₂ (ϵ = 9.08) solvent within the framework of the conductor like screening (COSMO) dielectric continuum approach.^[55] The relative energies were obtained from single-point calculations using the B3LYP^[56,57] functional together with the TZV/P^[52] basis set. They were computed from the gas-phase optimized structures as a sum of electronic energy, thermal corrections to free energy, and free energy of solvation. *g*-Tensors and hyperfine coupling constants were obtained from single-point calculations employing

the hybrid functional B3LYP functional.^[57,58] Scalar relativistic effects were included with ZORA paired with the SARC def2-TZVP(-f) basis sets^[58,59] and the decontracted def2-TZVP/J Coulomb fitting basis sets for all atoms. Increased integration grids (Grid4 and GridX4 in ORCA convention) and tight SCF convergence criteria were used in the calculation. The integration grids were increased to an integration accuracy of 11 (ORCA convention) for the metal center. Picture change effects were applied for the calculation of the hyperfine tensors. Optical properties were investigated with the Gaussian 09 program package (Revision A.02).^[60] Electronic transition energies and dipole moments were calculated employing time-dependent DFT (TD-DFT)^[60-62] using the hybrid functional B3LYP^[57,64] and the 6-311g* basis set. Solvent effects were included using the polarized continuum model (PCM)^[65-68] and at least 30 excited states were calculated in each case.

Synthesis: *4,6-Di-tert-butyl-2-(hydroxymethyl)aniline*: In a Paar pressure vessel, Pd/C (6.47 g, 20 mol%) was added to a solution of the 3,5-di-tert-butyl-2-nitrobenzaldehyde^[32] (4.00 g, 15.2 mmol) in CH₂Cl₂ (80 mL). The resulting suspension was stirred at RT under H₂ (25 bar) during 18 h. After complete consumption of the material (TLC monitoring) the mixture was filtrated through Celite and abundantly washed with CH₂Cl₂. The combined organic phase was dried over Na₂SO₄ and concentrated under reduced pressure to afford the title compound as a pale yellow oil (3.55 g, 99%). 2-(Hydroxymethyl)-4,6-di-tert-butylaniline was found to be air sensitive at room temperature and was used immediately in the next step without any further purification. ¹H NMR (400 MHz, CDCl₃): δ = 7.32 (d, *J* = 2.1 Hz, 1H), 7.02 (d, *J* = 2.1 Hz, 1H), 4.70 (s, 2H), 3.58 (brs, 3H), 1.48 (s, 9H), 1.32 ppm (s, 9H). ¹³C NMR (100 MHz, CDCl₃): δ = 141.8, 140.1, 133.8, 125.6, 124.6, 124.0, 65.6, 34.6, 34.2, 31.7, 30.1 ppm; IR: $\tilde{\nu}$ = 3493, 3376, 2955, 2867, 1625, 1477, 1363 cm⁻¹.

2-Amino-3,5-di-tert-butylbenzaldehyde: Freshly activated MnO₂ (2.22 g, 25.5 mmol, 23 equiv) was added to a solution of 2-(hydroxymethyl)-4,6-di-tert-butylaniline (261 mg, 1.1 mmol) in CH₂Cl₂ (5 mL). The resulting suspension was stirred at room temperature during 1 hour and filtrated through Celite. The Celite pad was abundantly rinsed with CH₂Cl₂ and the filtrate was concentrated under reduced pressure. The remaining material was purified by flash chromatography on silica gel (*c*-Hex/EtOAc; 9/1, v:v) to give the desired compound as a yellow solid (237 mg, 92%). ¹H NMR (300 MHz, CDCl₃): δ = 9.89 (s, 1H), 7.50 (d, *J* = 2.4 Hz, 1H), 7.33 (d, *J* = 2.4 Hz, 1H), 6.39 (brs, 2H), 1.45 (s, 9H), 1.32 ppm (s, 9H); ¹³C NMR (75 MHz, CDCl₃): δ = 195.0, 146.9, 138.3, 133.6, 130.6, 130.5, 119.0, 34.6, 34.2, 31.5, 29.7 ppm; IR: $\tilde{\nu}$ = 3525, 3316, 2955, 2870, 2727, 1657, 1581, 1546 cm⁻¹; MS (ESI): *m/z*: 264 [M+H]⁺; elemental analysis calcd (%) for C₁₅H₂₃NO: C, 77.21; H, 9.93; N, 6.00; found: C, 77.47; H, 9.55; N, 5.80.

(R,R)-N,N'-Bis(3,5-di-tert-butyl-2-aminobenzylidene)-1,2-diaminocyclohexane (H₂L1): A solution of 2-amino-3,5-di-tert-butylbenzaldehyde (100 mg, 0.43 mmol) and *(R,R)*-1,2-cyclohexanediamine (25 mg, 0.22 mmol, 0.5 equiv) in MeOH (2 mL) was heated at reflux for 1 hour. The resulting suspension was cooled to 5°C with an ice bath and the precipitate was filtered, washed with cold MeOH and dried under vacuum to afford the title compound (88 mg, 16 mmol) as a white solid. Yield: 75%. ¹H NMR (400 MHz, CDCl₃): δ = 8.33 (s, 2H), 7.25 (d, *J* = 1.5 Hz, 2H), 6.98 (d, *J* = 1.5 Hz, 2H), 6.78 (s, 4H), 3.22–3.29 (m, 2H), 1.92–1.96 (m, 2H), 1.86–1.88 (m, 2H), 1.69–1.77 (m, 2H), 1.46–1.54 (m, 2H), 1.43 (s, 18H), 1.24 ppm (s, 18H); ¹³C NMR (100 MHz, CDCl₃): δ = 164.7, 145.1, 137.4, 132.6, 128.6, 125.6, 117.9, 74.5, 34.7, 34.0, 33.7, 31.6, 29.9, 24.7 ppm; IR: $\tilde{\nu}$ = 3512, 3133, 2955, 2860, 1629, 1556, 1442, 1359 cm⁻¹; MS (ESI): *m/z*: 545.5 [M+H]⁺; elemental analysis calcd (%) for C₃₆H₅₆N₄: C, 79.36; H, 10.36; N, 10.28. Found: C, 79.03; H, 10.73; N, 10.22.

N,N'-Bis(3,5-di-tert-butyl-2-aminobenzylidene)-1,2-diaminoethane (H₂L2): L2 was prepared in an identical manner than H₂L1, using 1,2-diaminoethane instead of *(R,R)*-1,2-cyclohexanediamine. White solid, yield: 75%. ¹H NMR (400 MHz, DMSO): δ = 8.43 (s, 2H), 7.20 (d, *J* = 2.4 Hz, 2H), 7.09 (brs, 6H), 3.83 (s, 4H), 1.36 (s, 18H), 1.22 ppm (s, 18H). ¹³C NMR (100 MHz, DMSO): δ = 166.8, 144.8, 135.8, 131.7, 135.8, 131.7, 128.5, 125.1, 116.5, 61.6, 34.1, 33.5, 31.3, 29.2 ppm; IR: $\tilde{\nu}$ = 3398, 2952, 2905, 2867, 1632, 1477, 1461, 1359 cm⁻¹; MS (ESI): *m/z*: 491 [M+H]⁺; el-

emental analysis calcd (%) for C₃₂H₅₀N₄ 0.5(MeOH): C, 77.02; H, 10.34; N, 11.06; found: C, 76.86; H, 10.44; N, 10.82.

(R,R)-N,N'-Bis(3,5-di-tert-butyl-2-amidobenzylidene)-1,2-cyclohexanediaminonickel(II) (1): [Ni(OAc)₂]-4H₂O (27 mg, 0.11 mmol, 1.2 equiv) in methanol (8 mL) and triethylamine (50 μL, 0.36 mmol, 4 eq) was added to a solution of H₂L1 (50 mg, 0.09 mmol) in methanol (12 mL). The resulting solution was heated at reflux for 1 hour and the precipitate formed was collected by filtration, abundantly washed with cold methanol and dried under vacuum to afford a red solid (50 mg). Yield: 91%; IR: $\tilde{\nu}$ = 3436, 2952, 2867, 1603, 1540, 1442, 1363, 1150 cm⁻¹; MS (ESI): *m/z* = 601 [M+H]⁺; elemental analysis calcd (%) for C₃₆H₅₄N₄Ni: C 71.89, H 9.05, N 9.32; found: C 71.51, H 9.34, N 9.39.

N,N'-Bis(3,5-di-tert-butyl-2-amidobenzylidene)-1,2-ethylenediaminonickel(II) (2): Compound **2** was prepared analogously to H₂L1 from H₂L2 and [Ni(OAc)₂]-4H₂O; red solid, yield: 73%. MS (ESI): *m/z* = 547 [M+H]⁺; IR: $\tilde{\nu}$ = 3440, 2958, 2917, 2867, 1606, 1537, 1442, 1353 cm⁻¹; elemental analysis calcd (%) for C₃₂H₄₈N₄Ni-0.5(CH₃OH): C 69.28, H 8.94, N 9.94; found: C 69.07, H 9.07, N 9.86.

3: N-(3,5-Di-tert-butyl-2-amidobenzylidene)-N'-(3-tert-butyl-5-methoxysalicylidene)phenylene-1,2-diaminonickel(II) (3): [Ni(OAc)₂]-4H₂O (42 mg, 0.17 mmol) in MeOH (3 mL) was added to a yellow solution of *N*-(3-tert-butyl-5-methoxysalicylidene)phenylene-1,2-diamine (50 mg, 0.17 mmol) dissolved in MeOH (5 mL) was added. A solution of 2-amino-3,5-di-tert-butylbenzaldehyde (39 mg, 0.17 mmol) dissolved in MeOH (2 mL) and two equivalents of NEt₃ were immediately added to the red solution. The solution was stirred at room temperature for 1 h and the resulting precipitate was filtered, washed with cold MeOH and diethyl ether and dried under vacuum, giving a brown solid. Yield: 66%. ¹H NMR (CDCl₃, 400 MHz): δ = 8.44 (brs, 1H), 8.30 (brs, 1H), 7.75 (brs, 2H), 7.18 (brs, 3H), 7.07 (brs, 2H), 6.62 (brs, 2H), 3.79 (s, 3H), 1.52 (s, 9H), 1.47 (s, 9H), 1.34 (brs, 9H), NH not observed; IR: $\tilde{\nu}$ = 3421, 2943, 2905, 2867, 1603, 1575, 1534, 1359, 1198 cm⁻¹; MS (ESI): *m/z*: 570 [M+H]⁺; elemental analysis calcd (%) for C₃₃H₄₁N₃O₂Ni: C, 69.49; H, 7.25; N, 7.37; found: C, 69.30; H, 7.65; N, 7.24.

General protocol for the oxidation of complexes 1–3: Under argon, [AgSbF₆] (1.0 equiv) was added to a 0.05 M solution of the complex in anhydrous CH₂Cl₂. After stirring for 30 min at room temperature the mixture was filtered through a frit. Pentane was added to the remaining filtrate and the precipitate that formed was collected by filtration and dried.

[1]⁺[SbF₆]⁻: Brown solid, yield: 96%. IR: $\tilde{\nu}$ = 3402, 2939, 2870, 1581, 1363, 1245, 1122 cm⁻¹; MS (ESI): *m/z*: 600.5 [M-SbF₆]⁺; elemental analysis calcd (%) for C₃₆H₅₄N₄NiSbF₆·1.5(CH₂Cl₂): C, 46.69; H, 5.96; N, 5.81; found: C, 46.79; H, 5.94; N, 5.88.

[2]⁺[SbF₆]⁻: Brown solid, yield: 98%. IR: $\tilde{\nu}$ = 3411, 3392, 2962, 2870, 1575, 1363, 1245, 1163 cm⁻¹; MS (ESI): *m/z*: 546.5 [M-SbF₆]⁺; elemental analysis calcd (%) for C₃₂H₄₈N₄NiSbF₆·1.5(CH₂Cl₂): C, 44.19; H, 5.65; N, 6.15; found: C, 44.28; H, 5.34; N, 6.39.

[3]⁺[SbF₆]⁻: Brown solid, yield: 97%. IR: $\tilde{\nu}$ = 3354, 2958, 2905, 2870, 1600, 1575, 1549, 1530, 1363, 1201, 1119 cm⁻¹; MS (ESI): *m/z*: 570.4 [M-SbF₆]⁺; elemental analysis calcd (%) for C₃₃H₄₁N₃O₂NiSbF₆·1.5(CH₂Cl₂): C, 44.39; H, 4.75; N, 4.50; found: C, 44.78; H, 4.64; N, 4.83.

Acknowledgements

This work was supported by a doctoral fellowship (A. K.) from the DCM. We thank the Labex Arcane (Université Joseph Fourier, Grenoble) for financial support.

- [1] See the recent Special Issues of *Inorg. Chem.* on Redox-Active Ligands (**2011**, Vol. 50, Issue 20, Pages: 9737–9903) and *Eur. J. Inorg. Chem.* on Cooperative & Redox Non-Innocent Ligands in Directing Organometallic Reactivity (**2012**, Issue 3, Pages 340–580). See also excellent review articles: a) R. G. Hicks, *Org. Biomol. Chem.* **2007**, 5, 1321; b) S. Blanchard, E. Derat, M. Desage-El Murr, L. Fenster-

- bank, M. Malacria, V. Mourières-Mansuy, *Eur. J. Inorg. Chem.* **2012**, 376; c) W. Kaim, B. Schwederski, *Coord. Chem. Rev.* **2010**, 254, 1580.
- [2] a) K. G. Caulton, *Eur. J. Inorg. Chem.* **2012**, 435; b) C. R. Hess, T. Weyhermüller, E. Bill, K. Wieghardt, *Angew. Chem.* **2009**, 121, 3758; *Angew. Chem. Int. Ed.* **2009**, 48, 3703; c) M. M. Khusniyarov, T. Weyhermüller, E. Bill, K. Wieghardt, *J. Am. Chem. Soc.* **2009**, 131, 1208; d) N. Muresan, K. Chlopek, T. Weyhermüller, F. Neese, K. Wieghardt, *Inorg. Chem.* **2007**, 46, 5327; e) B. de Bruin, E. Bill, E. Bothe, T. Weyhermüller, K. Wieghardt, *Inorg. Chem.* **2000**, 39, 2936; f) A. C. Bowman, C. Milsman, C. C. H. Atienza, E. Lobkovsky, K. Wieghardt, P. J. Chirik, *J. Am. Chem. Soc.* **2010**, 132, 1676; g) J. M. Darmon, S. C. Stieber, K. T. Sylvester, I. Fernandez, E. Lobkovsky, S. P. Semproni, E. Bill, K. Wieghardt, S. DeBeer, P. J. Chirik, *J. Am. Chem. Soc.* **2012**, 134, 17125; h) S. K. Russell, A. C. Bowman, E. Lobkovsky, K. Wieghardt, P. J. Chirik, *Eur. J. Inorg. Chem.* **2012**, 535.
- [3] a) C. G. Pierpont, C. W. Lange, *Prog. Inorg. Chem.* **1994**, 41, 381; b) C. G. Pierpont, *Inorg. Chem.* **2011**, 50, 9766; c) P. Verma, J. Weir, L. Mirica, T. D. P. Stack, *Inorg. Chem.* **2011**, 50, 9816.
- [4] a) A. I. Poddel'sky, V. K. Cherkasov, G. A. Abakumov, *Coord. Chem. Rev.* **2009**, 253, 291; b) P. Chaudhuri, M. Hess, J. Müller, K. Hildenbrand, E. Bill, T. Weyhermüller, K. Wieghardt, *J. Am. Chem. Soc.* **1999**, 121, 9599; c) C. N. Verani, S. Gallert, E. Bill, T. Weyhermüller, K. Wieghardt, P. Chaudhuri, *Chem. Commun.* **1999**, 1747; d) H. Chun, C. N. Verani, P. Chaudhuri, E. Bothe, E. Bill, T. Weyhermüller, K. Wieghardt, *Inorg. Chem.* **2001**, 40, 4157; e) D. Herebian, P. Ghosh, H. Chun, E. Bothe, T. Weyhermüller, K. Wieghardt, *Eur. J. Inorg. Chem.* **2002**, 1957; f) H. Chun, P. Chaudhuri, T. Weyhermüller, K. Wieghardt, *Inorg. Chem.* **2002**, 41, 790; g) K. S. Min, T. Weyhermüller, K. Wieghardt, *Dalton Trans.* **2003**, 1126; h) K. S. Min, T. Weyhermüller, E. Bothe, K. Wieghardt, *Inorg. Chem.* **2004**, 43, 2922.
- [5] a) X. Ottenwaelder, R. Ruiz-Garcia, G. Blondin, R. Carrasco, J. Cano, D. Lexa, Y. Journaux, A. Aukauloo, *Chem. Commun.* **2004**, 504; b) X. Ottenwaelder, A. Aukauloo, Y. Journaux, R. Carrasco, J. Cano, B. Cervera, I. Castro, S. Curreli, C. Munoz, A. L. Rosello, B. Soto, R. Ruiz-Garcia, *Dalton Trans.* **2005**, 2516; c) K. Ray, T. Petrenko, K. Wieghardt, F. Neese, *Dalton Trans.* **2007**, 1552; d) R. Celenlilgil-Cetin, P. Paraskevopoulou, R. Dinda, N. Lalioti, Y. Sanakis, A. M. Rawashdeh, R. J. Staples, E. Sinn, P. Stravopoulos, *Eur. J. Inorg. Chem.* **2008**, 673; e) A. I. Nguyen, K. J. Blackmore, S. M. Carter, R. A. Zarkesh, A. F. Heyduk, *J. Am. Chem. Soc.* **2009**, 131, 3307; f) A. Kochem, O. Jarjays, B. Baptiste, C. Philouze, H. Vezin, K. Tsukidate, F. Tani, M. Orio, Y. Shimazaki, F. Thomas, *Chem. Eur. J.* **2012**, 18, 1068.
- [6] a) H. J. Krüger, *Angew. Chem.* **1999**, 111, 659; *Angew. Chem. Int. Ed.* **1999**, 38, 627; b) B. A. Jazdzewski, W. B. Tolman, *Coord. Chem. Rev.* **2000**, 200–202, 633; c) S. Itoh, M. Taki, S. Fukuzumi, *Coord. Chem. Rev.* **2000**, 198, 3; d) P. Chaudhuri, K. Wieghardt, *Prog. Inorg. Chem.* **2001**, 50, 151; e) F. Thomas, *Eur. J. Inorg. Chem.* **2007**, 2379; f) F. Thomas in *Stable Radicals: Fundamentals and Applied Aspects of Odd-Electron Compounds* (Ed.: R. G. Hicks), Wiley and Sons, Chichester, **2010**, p.281; g) Y. Shimazaki, O. Yamauchi, *Ind. J. Chem.* **2011**, 383; h) C. T. Lyons, T. D. P. Stack, *Coord. Chem. Rev.* **2013**, 257, 528.
- [7] a) J. W. Whittaker in *Metal Ions in Biological Systems, Vol. 30* (Eds.: H. Sigel, A. Sigel), Marcel Dekker, New York, **1994**, pp.315; b) C. D. Borman, C. G. Sellsell, A. Sokolowski, M. B. Twitchett, C. Wright, A. G. Sykes, *Coord. Chem. Rev.* **1999**, 190–192, 771; c) M. J. McPherson, M. R. Parsons, R. K. Spooner, C. M. Wilmot in *Handbook for Metalloproteins, Vol. 2* (Ed.: A. Messerschmidt, R. Huber, T. Poulos, K. Wieghardt), Wiley and Sons, Weinheim, **2001**, p.1272; d) J. W. Whittaker, *Adv. Protein Chem.* **2002**, 60, 1; e) J. W. Whittaker, *Chem. Rev.* **2003**, 103, 2347; f) M. S. Rogers, D. M. Dooley, *Curr. Opin. Chem. Biol.* **2003**, 7, 189; g) S. J. Firbank, M. Rogers, R. Hurtado-Guerrero, D. M. Dooley, M. A. Halcrow, S. E. V. Phillips, P. F. Knowles, M. J. McPherson, *Biochem. Soc. Trans.* **2008**, 31, 506.
- [8] a) K. M. Kadish, E. van Caemelbecke, G. Royal in *The Porphyrin Handbook, Vol. 8: Electron Transfers* (Eds.: K. M. Kadish, K. M. Smith, R. Guilard), Academic Press, London, **2000**, pp. 1–97; b) H. Li in *Handbook for Metalloproteins, Vol. 1* (Eds.: A. Messerschmidt, R. Huber, T. Poulos, K. Wieghardt), Wiley and Sons, Weinheim, **2001**, p.267; c) L. Que Jr., W. B. Tolman, *Nature* **2008**, 455, 333; d) J. Rittle, M. T. Green, *Science* **2010**, 330, 933; e) P. R. Ortiz de Montelano, *Chem. Rev.* **2010**, 110, 932.
- [9] a) J. L. Pierre, *Chem. Soc. Rev.* **2000**, 29, 251; b) P. J. Chirik, K. Wieghardt, *Science* **2010**, 327, 794; c) W. I. Dzik, J. I. van der Vlugt, J. N. H. Reek, B. de Bruin, *Angew. Chem.* **2011**, 123, 3416; *Angew. Chem. Int. Ed.* **2011**, 50, 3356; d) R. A. Luca, R. H. Crabtree, *Chem. Soc. Rev.* **2013**, 42, 1440.
- [10] a) W. Kaim, *Science* **2005**, 307, 216; b) R. G. Hicks, *Angew. Chem.* **2008**, 120, 7503; *Angew. Chem. Int. Ed.* **2008**, 47, 7393.
- [11] T. Buttner, J. Geier, G. Frison, J. Harmer, C. Cale, A. Schweiger, H. Schönberg, H. J. Grützmacher, *Science* **2005**, 307, 235.
- [12] E. T. Hennessy, T. A. Betley, *Science* **2013**, 340, 591.
- [13] Some representative reactions are: aromatic nucleophilic substitutions (P. R. Tentscher, S. N. Eustis, K. McNeill, J. S. Arey, *Chem. Eur. J.* **2013**, 19, 11216), addition to carbonyl (K. Sunggak, G. H. Joe, J. Y. Do, *J. Am. Chem. Soc.* **1993**, 115, 3328), N–H σ bond elimination to produce H₂ (T. Matsumoto, H. C. Chang, M. Wazizaka, S. Ueno, A. Kobayashi, A. Nakayama, T. Taketsugu, M. Kato, *J. Am. Chem. Soc.* **2013**, 135, 8646), C–C and C–N couplings (G. Bai, D. W. Stephan, *Angew. Chem.* **2007**, 119, 1888; *Angew. Chem. Int. Ed.* **2007**, 46, 1856. S. Wiese, J. L. McAfee, D. R. Pahls, C. L. McMullin, T. R. Cundari, T. H. Warren, *J. Am. Chem. Soc.* **2012**, 134, 10114); N–N couplings with diazo formation (A. Grirrane, A. Corma, H. Garcia, *Science* **2008**, 322, 1661) and N-hydroxylations by cyt. P450 (L. Ji, G. Schüürmann, *Angew. Chem. Int. Ed.* **2012**, 52, 744).
- [14] In contrast, *o*-phenylenediamine π radicals have been extensively studied; see Ref. [5].
- [15] a) R. Gross, W. Kaim, *Angew. Chem.* **1985**, 97, 869; *Angew. Chem. Int. Ed. Engl.* **1985**, 24, 856; b) K. Pohl, K. Wieghardt, W. Kaim, S. Steenken, *Inorg. Chem.* **1988**, 27, 440.
- [16] F. N. Penkert, T. Weyhermüller, E. Bill, P. Hildebrandt, S. Leconte, K. Wieghardt, *J. Am. Chem. Soc.* **2000**, 122, 9663.
- [17] Y. Miyazato, T. Wada, J. T. Muckerman, E. Fujita, K. Tanaka, *Angew. Chem.* **2007**, 119, 5830; *Angew. Chem. Int. Ed.* **2007**, 46, 5728.
- [18] a) D. Adhikari, S. Mossin, F. Basuli, J. C. Huffman, R. K. Szilagy, K. Meyer, D. J. Mindiola, *J. Am. Chem. Soc.* **2008**, 130, 3676; b) N. P. Mankad, W. E. Antholine, R. K. Szilagy, J. C. Peters, *J. Am. Chem. Soc.* **2009**, 131, 3878.
- [19] P. Maire, M. Königsmann, A. Sreekanth, J. Harmer, A. Schweiger, H. J. Grützmacher, *J. Am. Chem. Soc.* **2006**, 128, 6578.
- [20] E. Kogut, H. L. Wiencko, L. Zhang, D. E. Cordeau, T. H. Warren, *J. Am. Chem. Soc.* **2005**, 127, 11248.
- [21] E. R. King, E. T. Hennessy, T. A. Betley, *J. Am. Chem. Soc.* **2011**, 133, 4917.
- [22] X. Chen, X. Wang, Y. Sui, Y. Li, J. Ma, J. Zuo, X. Wang, *Angew. Chem. Int. Ed.* **2012**, 51, 11878.
- [23] P. M. Wojciechowski, W. Zierkiewicz, D. Michalska, P. Hobza, *J. Chem. Phys.* **2003**, 118, 10900.
- [24] a) M. Green, P. A. Tasker, *Chem. Commun.* **1968**, 518; b) M. Gerloch, M. Higson, E. D. McKenzie, *Chem. Commun.* **1971**, 1149; c) S. Busse, H. Elias, J. Fischer, M. Poggemann, K. J. Wannowius, *Inorg. Chem.* **1998**, 37, 3999; d) V. K. Sharma, O. P. Pandey, S. K. Sengupta, *Bull. Soc. Chim. Fr.* **1991**, 128, 469; e) G. Brewer, J. Jasinski, W. Mahany, L. May, S. Prytkov, *Inorg. Chim. Acta* **1995**, 232, 183; f) M. K. Taylor, J. Reglinski, D. Wallace, *Polyhedron* **2004**, 23, 3201.
- [25] B. M. Higson, E. D. M. McKenzie, *J. Chem. Soc. Dalton* **1972**, 269.
- [26] a) M. K. Taylor, J. Reglinski, L. E. A. Berlouis, A. R. Kennedy, *Inorg. Chim. Acta* **2006**, 359, 2455; b) J. Li, H. Song, C. Cui, J. P. Cheng, *Inorg. Chem.* **2008**, 47, 3468.
- [27] a) O. Rotthaus, O. Jarjays, F. Thomas, C. Philouze, C. Perez Del Valle, E. Saint-Aman, J. L. Pierre, *Chem. Eur. J.* **2006**, 12, 2293; b) O. Rotthaus, F. Thomas, O. Jarjays, C. Philouze, E. Saint-Aman,

- J. L. Pierre, *Chem. Eur. J.* **2006**, *12*, 6953; c) O. Rotthaus, O. Jarjayes, C. Perez del Valle, C. Philouze, F. Thomas, *Chem. Commun.* **2007**, 4462; d) O. Rotthaus, O. Jarjayes, C. Philouze, C. Perez Del Valle, F. Thomas, *Dalton Trans.* **2009**, 1792; e) H. Arora, C. Philouze, O. Jarjayes, F. Thomas, *Dalton Trans.* **2010**, 39, 10088; f) A. Kochem, M. Orio, O. Jarjayes, F. Neese, F. Thomas, *Chem. Commun.* **2010**, 46, 6765; g) L. Chiang, A. Kochem, O. Jarjayes, T. J. Dunn, H. Vezin, M. Sakaguchi, T. Ogura, M. Orio, Y. Shimazaki, F. Thomas, T. Storr, *Chem. Eur. J.* **2012**, *18*, 14117; h) A. Kochem, L. Chiang, B. Baptiste, C. Philouze, N. Leconte, O. Jarjayes, T. Storr, F. Thomas, *Chem. Eur. J.* **2012**, *18*, 14590; i) D. de Bellefeuille, M. S. Askari, B. Lassalle-Kaiser, Y. Journaux, A. Aukaaloo, M. Orio, F. Thomas, X. Ottenwaelder, *Inorg. Chem.* **2012**, *51*, 12796.
- [28] M. Orio, O. Jarjayes, H. Kanso, C. Philouze, F. Neese, F. Thomas, *Angew. Chem.* **2010**, *122*, 5109; *Angew. Chem. Int. Ed.* **2010**, *49*, 4989.
- [29] a) Y. Shimazaki, F. Tani, K. Fukui, Y. Naruta, O. Yamauchi, *J. Am. Chem. Soc.* **2003**, *125*, 10512; b) T. Storr, E. C. Wasinger, R. C. Pratt, T. D. P. Stack, *Angew. Chem.* **2007**, *119*, 5290; *Angew. Chem. Int. Ed.* **2007**, *46*, 5198; c) Y. Shimazaki, T. D. P. Stack, T. Storr, *Inorg. Chem.* **2009**, *48*, 8383.
- [30] a) Y. Shimazaki, T. Yajima, F. Tani, S. Karasawa, K. Fukui, Y. Naruta, O. Yamauchi, *J. Am. Chem. Soc.* **2007**, *129*, 2559; b) T. Storr, P. Verma, Y. Shimazaki, E. C. Wasinger, T. D. P. Stack, *Chem. Eur. J.* **2010**, *16*, 8980; c) Y. Shimazaki, N. Arai, T. J. Dunn, T. Yajima, F. Tani, C. F. Ramogida, T. Storr, *Dalton Trans.* **2011**, 40, 2469.
- [31] L. Benisvy, R. Kannapan, Y. Song, S. Milikisyants, M. Huber, I. Mutikainen, U. Turpeinen, P. Gamez, L. Bernasconi, E. J. Baerends, F. Hartl, J. Reedijk, *Eur. J. Inorg. Chem.* **2007**, 637.
- [32] I. Karamé, M. Jahjah, A. Messaoudi, M. L. Tommasino, M. Lemaire, *Tet. Assym.* **2004**, *15*, 1569.
- [33] H. J. Szatyłowicz, *J. Phys. Org. Chem.* **2008**, *21*, 897.
- [34] S. Di Bella, I. Fragala, *Eur. J. Inorg. Chem.* **2003**, 2606.
- [35] F. Thomas, O. Jarjayes, C. Duboc, C. Philouze, E. Saint-Aman, J. L. Pierre, *Dalton Trans.* **2004**, 2662.
- [36] N. Donati, D. Stein, T. Büttner, H. Schönberg, J. Harmer, S. Anadar-am, H. J. Grützmacher, *Eur. J. Inorg. Chem.* **2008**, 4691.
- [37] Y. Shimazaki, *Adv. Energy Mater. Adv. Mater. Phys. Chem.* **2013**, *3*, 60.
- [38] B. Speiser, A. Rieker, S. Pons, *J. Electroanal. Chem.* **1983**, *147*, 205.
- [39] a) R. S. Drago, E. I. Baucom, *Inorg. Chem.* **1972**, *11*, 2064; b) F. V. Lovecchio, E. S. Gore, D. H. Busch, *J. Am. Chem. Soc.* **1974**, *96*, 3109; c) H. J. Krüger, R. H. Holm, *Inorg. Chem.* **1987**, *26*, 3645; d) P. A. Connick, K. A. Macor, *Inorg. Chem.* **1991**, *30*, 4654; e) T. J. Collins, T. R. Nichols, E. S. Uffelman, *J. Am. Chem. Soc.* **1991**, *113*, 4708; f) F. Azevedo, M. A. Carrondo, B. De Castro, M. Convery, D. Domingues, C. Freire, M. T. Duarte, K. Nielsen, I. C. Santos, *Inorg. Chim. Acta* **1994**, *219*, 43; g) D. Pinho, P. Gomes, C. Freire, B. De Castro, *Eur. J. Inorg. Chem.* **2001**, 1483; h) Z. Xiao, B. O. Patrick, D. Dolphin, *Inorg. Chem.* **2003**, *42*, 8125–8127.
- [40] M. Green, P. A. Tasker, *J. Chem. Phys.* **1970**, 52–53, 2532.
- [41] F. Neese, *J. Biol. Inorg. Chem.* **2006**, *11*, 702.
- [42] C. Adamo, R. Subra, A. Di Matteo, V. Barone, *J. Chem. Phys.* **1998**, *109*, 10244.
- [43] G. N. R. Tripathi, Q. Sun, D. A. Armstrong, D. N. Chipman, R. H. Schuler, *J. Phys. Chem.* **1992**, *96*, 5344.
- [44] V. W. Manner, T. F. Markle, J. H. Freudenthal, J. P. Roth, J. M. Mayer, *Chem. Commun.* **2008**, 256.
- [45] K. Asami, K. Tsukidate, S. Iwatsuki, F. Tani, S. Karasawa, L. Chiang, T. Storr, F. Thomas, Y. Shimazaki, *Inorg. Chem.* **2012**, *51*, 12450.
- [46] TEXSAN, Crystal Structure Analysis Package, Molecular Structure, Corp., The Woodlands, TX, **1992**.
- [47] O. V. Dolomanov, L. J. Bourhis, R. J. Gildea, J. A. K. Howard, H. Puschmann, *J. Appl. Crystallogr.* **2009**, *42*, 339.
- [48] F. Neese, Wiley Interdiscip. Rev. Comput. Mol. Sci. **2012**, *2*, 73.
- [49] J. P. Perdew, *Phys. Rev. B* **1986**, *33*, 8822.
- [50] J. P. Perdew, *Phys. Rev. B* **1986**, *34*, 7406.
- [51] A. D. Becke, *Phys. Rev. A* **1988**, *38*, 3098.
- [52] A. Schäfer, C. Huber, R. Ahlrichs, *J. Chem. Phys.* **1994**, *100*, 5829.
- [53] F. Neese, *J. Comput. Chem.* **2003**, *24*, 1740.
- [54] F. Weigend, *Phys. Chem. Chem. Phys.* **2006**, *8*, 1057.
- [55] A. Klamt, G. Schürmann, *J. Chem. Soc. Perkin Trans. 2* **1993**, 799.
- [56] A. D. Becke, *J. Chem. Phys.* **1993**, *98*, 1372.
- [57] C. T. Lee, W. T. Yang, R. G. Parr, *Phys. Rev. B* **1988**, *37*, 785.
- [58] D. A. Pantazis, X. Y. Chen, C. R. Landis, F. Neese, *J. Chem. Theory Comput.* **2008**, *4*, 908.
- [59] D. A. Pantazis, F. Neese, *J. Chem. Theory Comput.* **2009**, *5*, 2229.
- [60] Gaussian 03, Revision A.02, M. J. Frisch, G. W. Trucks, H. B. Schlegel, G. E. Scuseria, M. A. Robb, J. R. Cheeseman, J. A. Montgomery, Jr., T. Vreven, K. N. Kudin, J. C. Burant, J. M. Millam, S. S. Iyengar, J. Tomasi, V. Barone, B. Mennucci, M. Cossi, G. Scalmani, N. Rega, G. A. Petersson, H. Nakatsuji, M. Hada, M. Ehara, K. Toyota, R. Fukuda, J. Hasegawa, M. Ishida, T. Nakajima, Y. Honda, O. Kitao, H. Nakai, M. Klene, X. Li, J. E. Knox, H. P. Hratchian, J. B. Cross, C. Adamo, J. Jaramillo, R. Gomperts, R. E. Stratmann, O. Yazyev, A. J. Austin, R. Cammi, C. Pomelli, J. W. Ochterski, P. Y. Ayala, K. Morokuma, G. A. Voth, P. Salvador, J. J. Dannenberg, V. G. Zakrzewski, S. Dapprich, A. D. Daniels, M. C. Strain, O. Farkas, D. K. Malick, A. D. Rabuck, K. Raghavachari, J. B. Foresman, J. V. Ortiz, Q. Cui, A. G. Baboul, S. Clifford, J. Cioslowski, B. B. Stefanov, G. Liu, A. Liashenko, P. Piskorz, I. Komaromi, R. L. Martin, D. J. Fox, T. Keith, M. A. Al-Laham, C. Y. Peng, A. Na-nayakkara, M. Challacombe, P. M. W. Gill, B. Johnson, W. Chen, M. W. Wong, C. Gonzalez, J. A. Pople, Gaussian, Inc., Pittsburgh, PA, **2003**.
- [61] M. E. Casida in *Recent Advances in Density Functional Methods* (Ed.: D. P. Chong), World Scientific, Singapore, **1995**.
- [62] R. E. Stratmann, G. E. Scuseria, M. J. Frisch, *J. Chem. Phys.* **1998**, *109*, 8218.
- [63] R. Bauernschmitt, R. Ahlrichs, *Chem. Phys. Lett.* **1996**, *256*, 454.
- [64] P. J. Stephens, F. J. Devlin, C. F. Chabalowski, M. J. Frisch, *J. Phys. Chem.* **1994**, *98*, 11623.
- [65] V. Barone, M. Cossi, J. Tomasi, *J. Chem. Phys.* **1997**, *107*, 3210.
- [66] V. Barone, M. Cossi, J. Tomasi, *J. Comput. Chem.* **1998**, *19*, 404.
- [67] S. Miertus, E. Scrocco, J. Tomasi, *J. Chem. Phys.* **1981**, *74*–75, 117.
- [68] J. Tomasi, B. Mennucci, E. Cancès, *J. Mol. Struct.* **1999**, *474*–515, 211.

Received: August 15, 2013

Published online: November 4, 2013